

RESEARCH

Open Access



A dual-targeting bio-liposomes nanodrug repair endothelial cell dysfunction and restore macrophage cholesterol flow homeostasis to treat early atherosclerosis

Qi Zhang^{1,2†}, Shengchao Ma^{1,2†}, Xue Kang⁴, Yi Liu^{2,5}, Fei Ma^{2,5}, Feifei Yu^{2,5}, Xiaolan Luo^{1,2}, Guizhong Li^{2,5}, Yinju Hao^{2,6}, Huiping Zhang^{6,7*}, Bin Liu^{2,3*} and Yideng Jiang^{2,5*}

Abstract

Hyperhomocysteinemia (HHy) can lead to vascular endothelial cell dysfunction, progressive inflammation and lipid metabolism disorder, which finally result in the onset and development of atherosclerosis, a major contributor to cardiovascular diseases. Given the complexity of pathological process, treatments based on a single target often showed limited therapeutic efficacy against AS. Thus, developing nanodrug for enhanced multi-targets therapy is promising. In this study, we constructed a dual-targeting nanodrug (HA-ML@ES NPs) co-loaded with Shikonin (SKN) and Evolocumab (Evol). In vitro results showed that HA-ML@ES NPs could simultaneously target dysfunctional endothelial cell and inflammatory macrophage through the interaction between HA and CD44. In vivo assay indicated that HA-ML@ES NPs with long circulation and plaque accumulation efficiently attenuate endothelial cell dysfunction by inhibiting glycolysis and restore cholesterol flow homeostasis in macrophage by reprogramming macrophage phenotype, which finally attenuated the development of atherosclerosis. Collectively, these results present a highly promising dual-cell therapeutic approach based on HA-ML@ES NPs for the management of early atherosclerosis.

Keywords Atherosclerosis, Shikonin, Evolocumab, Endothelial cells dysfunction, Cholesterol flow homeostasis

[†]Qi Zhang and Shengchao Ma contributed equally to this work.

*Correspondence:

Huiping Zhang

zhp19760820@163.com

Bin Liu

binliu2001@hotmail.com

Yideng Jiang

iydeng@nxmu.edu.cn

¹School of Inspection, Ningxia Medical University, Yinchuan 750004, China

²NHC Key Laboratory of Metabolic Cardiovascular Diseases Research, Ningxia Medical University, Yinchuan 750004, China

³College of Biology, Hunan University, Changsha 410082, China

⁴Department of Clinical Medicine, Ningxia Medical University, Yinchuan 750004, China

⁵School of Basic Medical Sciences, Ningxia Medical University, Yinchuan 750004, China

⁶Medical Experimental Center, General Hospital of Ningxia Medical University, Yinchuan 750004, China

⁷Department of Medical Genetics, Hunan Provincial Maternal and Child Health Hospital, Changsha 410008, China



© The Author(s) 2025. **Open Access** This article is licensed under a Creative Commons Attribution-NonCommercial-NoDerivatives 4.0 International License, which permits any non-commercial use, sharing, distribution and reproduction in any medium or format, as long as you give appropriate credit to the original author(s) and the source, provide a link to the Creative Commons licence, and indicate if you modified the licensed material. You do not have permission under this licence to share adapted material derived from this article or parts of it. The images or other third party material in this article are included in the article's Creative Commons licence, unless indicated otherwise in a credit line to the material. If material is not included in the article's Creative Commons licence and your intended use is not permitted by statutory regulation or exceeds the permitted use, you will need to obtain permission directly from the copyright holder. To view a copy of this licence, visit <http://creativecommons.org/licenses/by-nc-nd/4.0/>.

Introduction

Hyperhomocysteinemia (HHcy) induced Atherosclerosis (AS) is a chronic, multi-factorial disease that tightly related with Endothelial cells dysfunction, progressive inflammation, and disturbed lipid metabolism [1, 2]. Endothelial cell apoptosis is recognized as a key “initiation point” for the progression of endothelial dysfunction and the development of atherosclerotic plaques [3, 4]. Moreover, endothelial barrier damage and the widening of intercellular spaces promote the infiltration of circulating lipoprotein particles into the vascular wall and enhance foam cell formation. Inflammatory factors secreted from foam cell further accelerate the progression of atherosclerosis by forming inflammatory environment [5]. Therefore, inhibition of endothelial cells apoptosis and regulation of lipid metabolism is expected to be an effective program for the treatment of atherosclerosis.

Shikonin (SKN), the active components of *Lithospermum erythrorhizon* with antioxidant and anti-inflammatory function can inhibit endothelial cell apoptosis to improve endothelial cell dysfunction [6, 7]. However, due to the complicated pathologic mechanisms of AS, sole drug therapy is difficult to achieve effective inhibition of atherosclerotic plaques. Evolocumab (Evol), a specific inhibitor of the proprotein convertase subtilisin/Kexin type 9 (PCSK9), is currently the most effective drug for the treatment of cardiovascular disease in clinical practice [8, 9]. This drug can effectively inhibit inflammatory response and foam cell formation [10]. Therefore, it is reasonable to hypothesize that the combination of SKN and Evol could treat atherosclerosis by inhibiting endothelial cell apoptosis, inflammatory response and regulating cholesterol flow homeostasis.

However, the short circulation time, nonspecific distribution, and low drug utilization of oral SKN have severely hindered its clinical application [11]. Recently, more and more nanodrug delivery systems have been developed to address these challenges with satisfied results [12]. Among these nanomaterials, liposome nanoparticles (L NPs) have been used as drug carrier for the treatment of AS [13]. Moreover, the hybridization of liposomes with macrophage membranes (M ϕ m) efficiently extended half-life time and enhanced immune escape ability during blood circulation [14]. In addition, the disruption of intercellular continuity as well as the increase of cellular gaps in the atherosclerotic plaques provide a natural pathway for the accumulation of nanoparticles [15].

In this study, we designed and developed nanomedicines for the purpose of actively targeting atherosclerotic plaques using liposomes loaded with both Evol and SKN. The liposome nanoparticles were fused with M ϕ m to extend the circulating half-life of the drug. HA-PEG₂₀₀₀-DSPE attaching on the surface of ML@ES NPs endowed targeting ability to endothelial and macrophage cells via

HA and CD44 interaction. The modification of M ϕ m and HA enabled the nanoparticles to extend drug half-life, target atherosclerotic plaques. This controllable release nanomedicine can be used for efficient treatment of HHcy-induced early atherosclerosis via repairing endothelial damage and regulating lipid metabolism of macrophages (Scheme 1).

Materials and methods

Materials

Shikonin was supplied by Chengdu Pufei De Biotech Co. Ltd (China). Evolocumab provided by Amgen Manufacturing Limited (USA). Homocysteine (Hcy) was acquired from Sigma-Aldrich (H462, USA) L-Alpha-phosphatidyl choline (SPC) and cholesterol were purchased from Shanghai Ryon Bio-logical Technology Co. Ltd (Shanghai, China). DSPE-PEG₂₀₀₀-NH₂ was obtained from Ponsure Inc (Shanghai China).

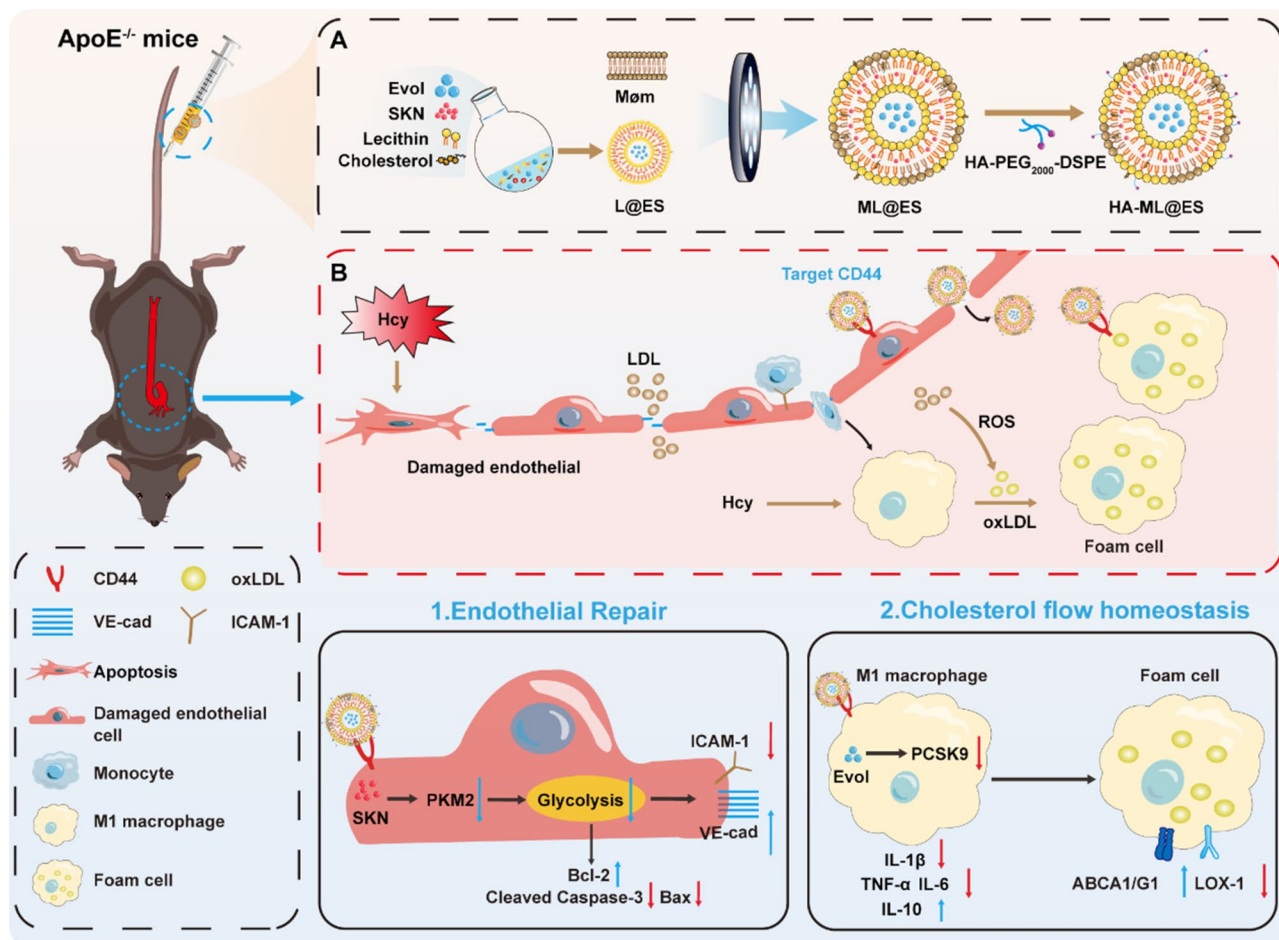
Synthesis of HA-ML@ES NPs

M ϕ m were isolated from RAW264.7 cells as described previously [16]. First, 2.0×10^7 RAW264.7 cells were resuspended in pre-cooled extraction reagent (1 mL) containing PMSF (1 mM and lysed at 4 °C for 30 min. Subsequently frozen and thawed at -80 °C and 25 °C were repeated four times, respectively, before the supernatant was collected by centrifugation. Subsequently, the collected supernatant was centrifuged at 13000 rpm for 30 min at 4 °C, and the remaining precipitate was M ϕ m. The total protein of M ϕ m was quantitatively analyzed afterwards.

L@ES NPs were prepared using reverse evaporation. Lecithin, cholesterol, SKN and Evol (mass ratio 20:10:3:5) were dissolved in a solution of a mixture of chloroform (4 mL) and ether (6 mL), followed by the addition Double Distilled Water (ddH₂O) (4 mL), and sonicated in a water bath to form a W/O emulsion. This was followed by evaporation under reduced pressure, after which 10 mL of PBS was added to the gelation solution, and rotary evaporation was continued at 37 °C to remove residual organic solvents and to dissolve the gel to form an emulsion nano-liposome suspension, which was then dialyzed for 12 h to remove free Evol and SKN using a 300 kDa dialysis bag. To the L@ES NPs solution, M ϕ m (2 mg) was added, stirred in a water bath at 37 °C for 1 h. Uniformly sized ML@ES NPs were obtained by extruding them through a polyethersulfone membrane (0.22 μ m). Finally, Combining HA-PEG₂₀₀₀-DSPE with ML@ES NPs to form HA-ML@ES NPs.

Characterization of nanoparticles

Transmission electron microscopy (TEM) was used to observe the morphological features of L@ES NPs and HA-ML@ES NPs. The size of the nanodrugs and the Zeta



Scheme 1 Preparation diagram of HA-ML@ES NPs and treatment strategy of atherosclerosis

potential were studied using Dynamic light scattering (DLS) (Nano ZS90 Zetasizer, Malvern).

The proteins from Mømembrane and ML@ES NPs were extracted by using Membrane Protein Extraction Reagent, and the extracted protein samples were subjected to gel electrophoresis and stained with Coomassie Brilliant Blue to study the integrity of the membrane proteins on HA-ML@ES NPs, and the membrane specific molecule CD68 was verified by Western blot.

Förster resonance Energy transfer (FRET) and membrane fusion confocal images were used to study fusion efficiency of L@ES NPs and Mømembrane by first labeling L@ES NPs with both DiD and Dil dyes, and then adding Mømembrane and stirring at 37 °C for 1 h to promote fusion. The DiD and Dil labeled L@ES NPs were used as a control, and the signal changes were detected on a fluorescence spectrophotometer by detecting the Dil (564 nm) signal changes. Using Dil-labeled L@ES and DiO-labeled Mømembrane, the L NPs and Mømembrane were mixed according to the mass ratio of lecithin/Mømembrane = 10/1 and stirred at 37 °C for 1 h in a dark environment to fully fuse the L NPs and Mømembrane, followed by observation of the fusion using confocal microscopy.

To study the stability of the prepared HA-ML@ES NPs in PBS and 10% FBS solutions, the prepared HA-ML@ES NPs were dissolved in PBS and 10% FBS solutions, respectively, and were detected on days 1, 2, 3, 4, 5, 6, and 7 using a Nano ZS90 Zetasizer (Malvern) DLS to detect the size change of nanoparticles.

To study the release behavior of Evol and SKN from L@ES NPs and HA-ML@ES NPs at PBS (pH = 7.4), these nanodrugs were incorporated into dialysis membranes with molecular weight limits of 300 kDa and 3500 Da. These membranes were then submerged in a 50 mL PBS buffer solution and agitated within a water bath maintained at 37 °C. At specified intervals, solution (1 mL) was withdrawn and replenished with PBS (1 mL). The released Evol and SKN compounds were gathered from the eluate; Evol concentrations were quantified using the BCA Protein Assay Kit, whereas SKN levels were measured with a UV-Vis spectrophotometer (model UV-1800, Shimadzu Corporation, Japan).

In vitro blood compatibility

In hemolysis experiments, red blood cells (RBCs) were harvested from C57BL/6 mice. 5% A suspension of RBCs at a concentration of 5% (v/v in PBS) was exposed to varying doses of HA-ML@ES NPs, specifically at different concentrations (0, 1.2, 2.4, and 4.8 $\mu\text{g mL}^{-1}$). HA-ML@ES NPs and ddH₂O group at 37 °C for 4 h. Subsequently, the shape of the erythrocytes was examined using an inverted microscope, and after centrifugation at 3500 rpm for 5 min, the supernatant was taken and the absorbance was measured by a microtiter plate detector at 562 nm. The erythrocytes treated with ddH₂O were used as the positive group, and the hemoglobin release rate was set at 100%. In the coagulation assay, platelet-rich plasma (PRP) was obtained from C57BL/6 mice. PRP was co-incubated with Evol+SKN (1.25 nM+250 nM), HA-ML@ES NPs (4.8 $\mu\text{g}\cdot\text{mL}^{-1}$) and thrombin (100 $\mu\text{g}\cdot\text{mL}^{-1}$) for 1 h at 37 °C, and the absorbance was measured at 650 nm using a microplate detector.

Zebrafish co-incubation toxicity assay

Zebrafish eggs were co-cultured with different concentrations (0, 1.2, 2, 4, 4.8 $\mu\text{g}\cdot\text{mL}^{-1}$) of HA-ML@ES NPs, and the morphology of zebrafish on days 0, 1, 2, and 6 and the heartbeat and length of the body on day 6 were observed by inverted microscope, respectively.

Cell culture

RAW264.7, HUVEC, VSMC, and H9C2 were obtained from the cell bank of the Chinese Academy of Sciences. These cells were cultured in DMEM medium (Gibco, USA) supplemented with 10% fetal bovine serum (Gibco) and 1% penicillin and streptomycin (Invitrogen, USA) at 37 °C in a 5% CO₂ incubator.

In vitro cytotoxicity evaluation

H9C2, HUVEC, VSMC, and RAW264.7 cells were seeded into 96-well plates at a density of 5,000 cells per well and incubated until they reached approximately 90% confluence. Various concentrations of HA-ML@ES NPs, specifically 0, 1.2, 2.4, and 4.8 $\mu\text{g}\cdot\text{mL}^{-1}$, were added to the cultures and incubated for a period of 24 h. After replacing the fresh medium, 10 μL (0.5 $\text{mg}\cdot\text{mL}^{-1}$) of MTT reagent was added to each well and incubated for another 2 h. The absorbance was then measured at 490 nm.

CD44 expression

HUVECs and RAW264.7 were inoculated into 24-well and 6-well plates, respectively. Both types of cells were co-incubated with (0,100 μM) Hcy for 24 h, respectively. The medium from the 24-well plates was removed, followed by three washes with PBS. Cells were then fixed with a 4% paraformaldehyde solution for 30 min, and closed in 5% goat serum for 30 min before addition of a

primary antibody targeting CD44 (15675-1-AP, 1:300, Proteintech) and incubation at 4 °C overnight. After washing 3 times, rabbit secondary antibody was incubated for 2 h. In addition, staining with DAPI (Solarbio, China) before observation using a Confocal Laser Scanning Microscopy (CLSM) (Ti-E + A1 MP, Japan).

Immune escape and cell uptake by confocal laser scanning microscopy

In immune escape experiments, Dil-labeled L@ES NPs, ML@ES NPs, and HA-ML@ES NPs were added into 24-well plates inoculated with macrophages inside the culture for 4 h, and after fixation with 4% paraformaldehyde for 30 min, they were stained using DAPI for 6 min, and observed by using CLSM.

In the cell uptake assay, HUVECs and RAW264.7 were inoculated into 24-well plates so that the number of cells per well was about 5×10^4 , respectively, and were incubated with different concentrations (0, 100 μM) of Hcy for 24 h. After replacing the 1% FBS medium, one of the groups was first incubated with 500 ($\mu\text{g}\cdot\text{mL}^{-1}$) HA for 30 min, and all the groups were incubated with 100 $\mu\text{g}\cdot\text{mL}^{-1}$ Dil-labeled HA-ML@ES was co-incubated for 4 h, and the cells were fixed with 4% paraformaldehyde and stained with DAPI for 6 min, and observed using CLSM.

Mimicking the AS plaque microenvironment using a co-culture model. HUVECs were cultured in the upper chamber, while RAW264.7 cells were placed in the bottom chamber. After a 24 h treatment with Hcy (100 μM), Dil-labeled L@ES NPs or HA-ML@ES NPs were introduced into the upper chamber and incubated for 4 h. Following this, the cells were rinsed three times with PBS, fixed with 4% paraformaldehyde, and stained with DAPI prior to examination under CLSM.

Cell uptake by flow cytometry

In cell uptake experiments, HUVECs and RAW264.7 cells were inoculated into 6-well plates to make the number of cells per well about 2×10^5 , respectively, and incubated with different concentrations (0, 100 μM) of Hcy for 24 h. After replacing the 1% FBS medium, one group was firstly added with HA (500 $\mu\text{g}\cdot\text{mL}^{-1}$) and incubated for 30 min, and one group in 0 μM Hcy was added with PBS as Control, and all the remaining groups were co-incubated with Dil-labeled (100 $\mu\text{g}\cdot\text{mL}^{-1}$) HA-ML@ES NPs for 4 h. Cells were collected by centrifugation and intracellular fluorescence was detected and analyzed by flow cytometry.

RNA sequencing and bioinformatics analysis

HUVECs were seeded in 6-well plates. We cultured cells with Evol+SKN and HA-ML@ES NPs (Evol: 1.25 nM, SKN: 250 nM) for 2 h, we then treating HUVECs with

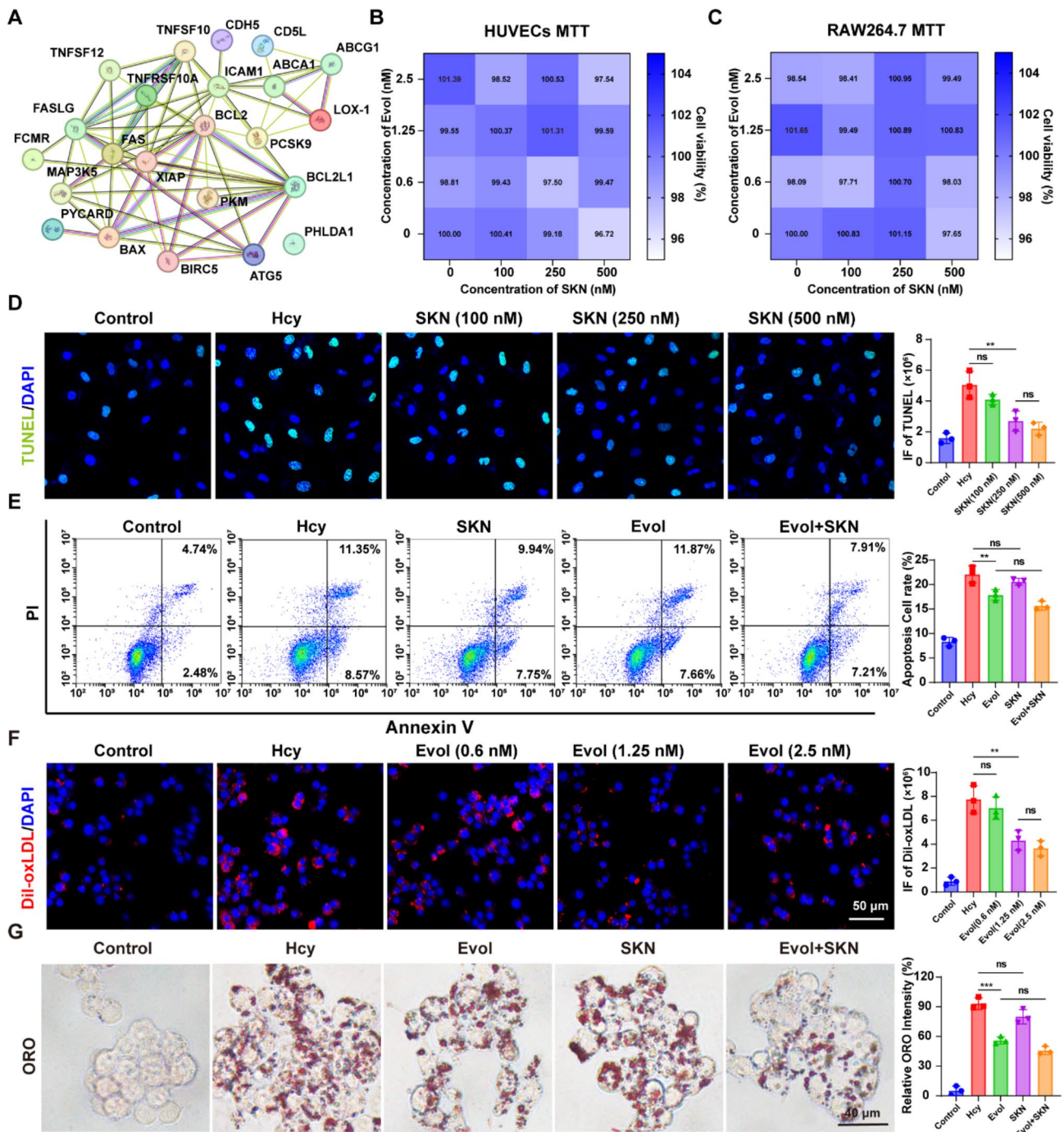


Fig. 1 SKN inhibits apoptosis of HUVECs and Evol inhibits RAW264.7 lipid influx. **(A)** Protein-protein interaction network analysis among the 23 potential intersection targets. **(B)** Cell viability of HUVECs and **(C)** RAW264.7 cells with SKN and Evol co-treatment. **(D)** Confocal images and quantitative analysis of TUNEL staining in HUVECs. Scale bar = 50 μ m. [Hcy] = 100 μ M. **(E)** Flow cytometry analysis of apoptosis of activated HUVECs (left) with quantitative data (right). [Hcy] = 100 μ M. **(F)** Confocal images and quantitative analysis of Dil-oxLDL in RAW264.7 with different treatment. [Hcy] = 100 μ M, [Dil-oxLDL] = 40 μ g/mL. Scale bar = 50 μ m. **(G)** images of Oil Red O (ORO)-stained in RAW264.7 cells. [Hcy] = 100 μ M, [oxLDL] = 80 μ g/mL. Scale bar = 20 μ m. Data are mean \pm SD ($n=3$) ** $P < 0.01$, *** $P < 0.001$

100 μ M Hcy for 24 h. After that, cells were collected and total RNA was extracted using Trizol reagent. mRNA sequencing program was performed at Guangzhou Kidio Co. Ltd (Guangzhou, China). After establishing

the sequencing library, the results were analyzed using an online analysis website (<https://www.omicstudio.com/analysis/>). Principal component analysis (PCA) was performed using the principal component function of R

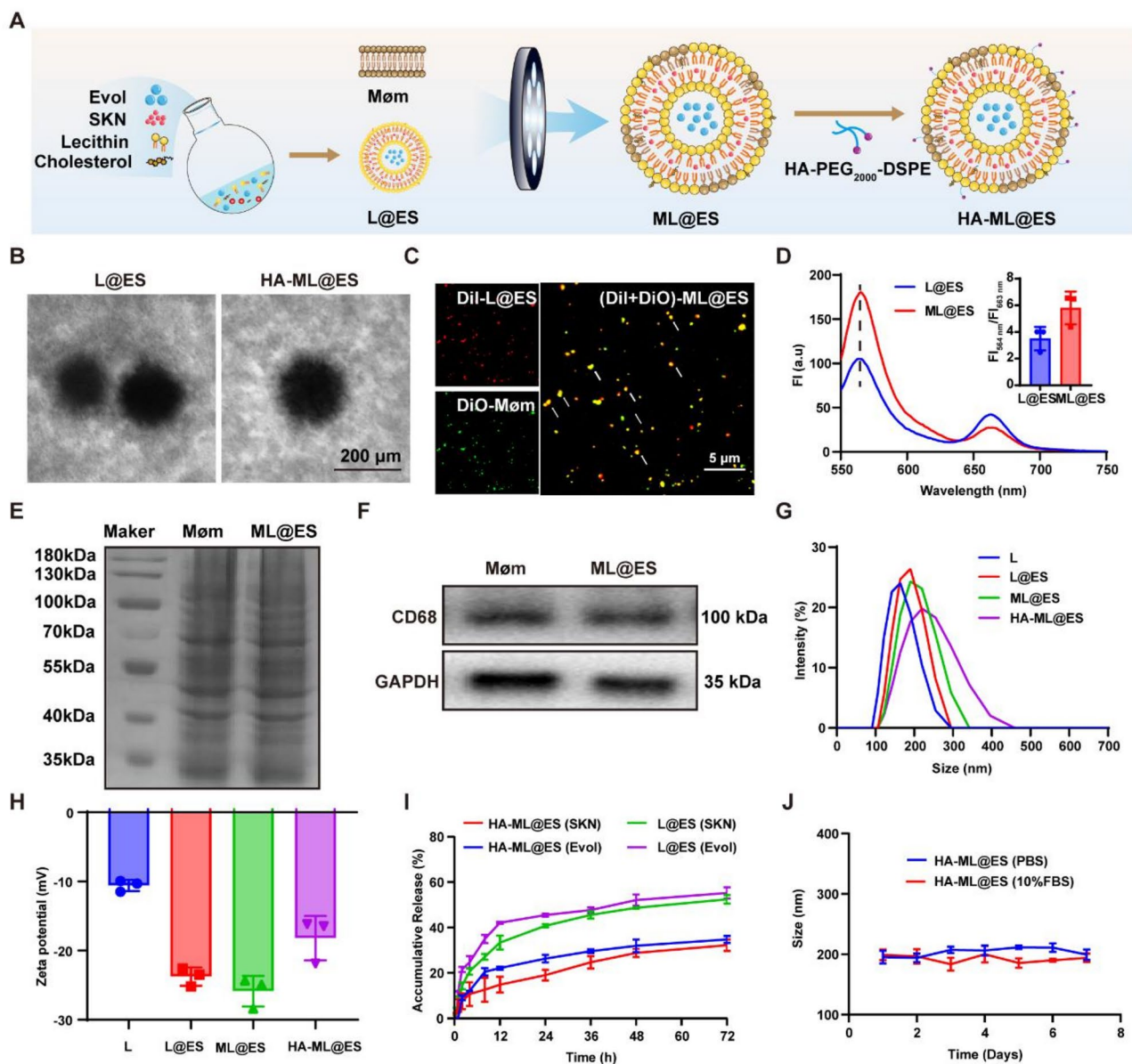


Fig. 2 Characterization of HA-ML@ES NPs. **(A)** HA-ML@ES NPs synthesis pattern diagram. **(B)** TEM image of L@ES NPs and HA-ML@ES NPs. **(C)** CLSM imaging of ML@ES NPs. Scale bar = 5 μm . **(D)** Fusion efficiency analysis of Mø and ML@ES NPs by FRET. **(E)** SDS-PAGE protein profile of Mø and ML@ES NPs. **(F)** Western blot analysis of Mø and ML@ES NPs protein marker CD68. **(G)** Particle size and **(H)** Zeta potential analysis of L, L@ES NPs, ML@ES NPs, and HA-ML@ES NPs by DLS. **(I)** Cumulative SKN and Evol release from L@ES NPs and HA-ML@ES NPs at PBS (pH 7.4). **(J)** The stability of HA-ML@ES NPs in in PBS and DMEM containing 10% FBS, over 7 days

(<http://www.r-project.org/>). Functional enrichment analysis was performed using the R package cluster Profiler based on the KEGG database.

In vitro HA-ML@ES NPs restore HUVECs dysfunction by inhibiting Glycolysis

Apoptosis analysis

HUVECs were seeded in 6-well plates. We cultured cells with Evol+SKN and HA-ML@ES NPs (Evol:1.25 nM, SKN:250 nM) for 2 h, we then treating HUVECs with Hcy (100 μM) for 24 h, the apoptosis rate in HUVECs

was evaluated via flow cytometry using V-FITC and PI staining. Following this, the treated cells were lysed, and the extracted total proteins were resolved on SDS-PAGE gels. Proteins were subsequently transferred onto PVDF membranes. These membranes were blocked using TBST buffer with 5% non-fat milk and incubated overnight at 4 $^{\circ}\text{C}$ with primary antibodies against cleaved caspase-3 (66470-2-IG, 1:2000, Proteintech), Bcl-2 (68103-1-IG, 1:20000, Proteintech), BAX (50599-2-IG, 1:3000, Proteintech), and β -actin (20536-1-AP, 1:3000, Proteintech). Post-incubation, the membranes were rinsed and further

incubated with secondary antibodies for 2 h at room temperature. Lastly, after washing, the protein bands were detected using chemiluminescence imaging system.

HUVECs adhesion function assay

HUVECs were inoculated in 24-well plates. Before stimulation with Hcy (100 μ M) for 24 h, Evol + SKN and HA-ML@ES NPs (Evol: 1.25 nM, SKN: 250 nM) were added to the wells for 2 h. After 1 h of 5% goat serum containment, primary antibody of ICAM-1 (10831-1-AP, 1:400, Proteintech) and VE-cad (20874-1-AP, 1:250, Proteintech) was incubated overnight at 4 °C. After washing three times with PBST, fluorescent rabbit secondary antibody was incubated for 2 h. Cell nuclei were stained with DAPI before observation using CLSM.

Glycolytic function assay for HUVECs

The Seahorse XF 24 – 3 analyzer (Agilent, USA) was used to determine the glycolysis stress assay (extracellular acidification rate, ECAR). HUVECs were plated onto cell culture microplates (2,000 cells/well) in DMEM with 10% FBS and cultured cells with Evol + SKN and HA-ML@ES NPs (Evol:1.25 nM, SKN:250 nM) for 2 h, we then treating HUVECs with Hcy (0 or 100 μ M) for 24 h. To allow the cells to equilibrate with the assay medium, they were incubated at 37 °C in a CO₂-free XF prep station for 1 h before the Seahorse assay. In the glycolysis stress test, after properly plating and treating HUVECs as described above, 10 mM glucose, 1 μ M oligomycin, and 50 mM 2-deoxy-D-glucose (2-DG glycolysis inhibitor) were sequentially supplied according to the XF Cell Glycolysis Stress Test Kit (Agilent, USA). Finally, the values obtained were normalized by cell staining and counting.

HUVECs were inoculated in 6-well and 96-well plates. After stimulation with Evol + SKN and HA-ML@ES NPs (Evol:1.25 nM, SKN:250 nM) for 2 h. We then treating HUVECs with Hcy (100 μ M) for 24 h. Intracellular ATP, L-lactate and lactate dehydrogenase contents were determined according to the kit instructions (Beyotime, S0026, S0208S and C0016), respectively.

After washing HUVECs with PBST, PKM2 (15822-1-AP, 1:200, Proteintech) primary antibody was incubated overnight. After three additional PBST washes, FITC-secondary antibody was incubated. Prior to observation under CLSM, nuclei were stained with DAPI.

In vitro inhibit lipid influx and cholesterol efflux of HA-ML@ES NPs

After incubation with Hcy (100 μ M) for 24 h, RAW264.7 cells were further treated with Evol + SKN and HA-ML@ES NPs, both at the same concentration of Evol (1.25 nM) and SKN (250 nM), followed by the addition of oxLDL (80 μ g mL⁻¹) and incubated for 48 h. After incubation, RAW264.7 cells were further stained with 3% ORO.

The effects of HA-ML@ES NPs on intracellular levels of PCSK9 protein, lipid uptake receptor protein LOX-1 and cholesterol efflux-associated protein ABCA1/G1 were then assessed. After treatment, appeal cells were lysed and the total proteins were harvested for subsequent evaluation. The levels of PCSK9 (55206-1-AP, 1:2500, Proteintech), LOX-1 (11837-1-AP, 1:3000, Proteintech), ABCA1 (26564-1-AP, 1:1000, Proteintech) and ABCG1 (13578-1-AP, 1:4000, Proteintech) were assessed using Western blot. The protein expression of ABCA1 (26564-1-AP, 1:300, Proteintech) and ABCG1 (13578-1-AP, 1:500, Proteintech) were also observed using CLSM.

In vitro anti-inflammatory effects of HA-ML@ES NPs

RAW264.7 were inoculated in 24-well plates. After stimulation with Evol + SKN and HA-ML@ES NPs (Evol: 1.25 nM, SKN: 250 nM) for 2 h. We then treating HUVECs with 100 μ M Hcy for 24 h. IL-1 β , IL-6, TNF- α , and IL-10 levels in supernatants were measured using the Elisa kit instructions (QuantiCyto, EMC001b, EMC004, EMC102a, EMC005).

In the study of macrophage M1/M2 phenotypic transformation experiment, 2×10^5 RAW264.7 were inoculated into 6-well plates. After stimulation with Evol + SKN and HA-ML@ES NPs (Evol: 1.25 nM, SKN: 250 nM) for 2 h. We then treating HUVECs with 100 μ M Hcy for 24 h. The cells were closed with Fc for 15 min. After that, PE-CD80 (Biolegend, USA, 1:100) staining was added for 30 min, followed by 0.3% triton to break the membrane for 20 min, and then FITC-CD206 (Santa Cruz, USA, 1:50) staining was added for 30 min. Intracellular fluorescence was detected and analyzed by flow cytometry.

Pharmacokinetics and targeting ability

We utilized Ce6 and HA-ML@ES^{Ce6} nanoparticles to evaluate their half-life, biodistribution, and aggregation characteristics within mice. Briefly, blood samples from Kunming mice were collected at different time points (0, 1, 2, 4, 8, 14, and 24 h) by intravenous injection of Ce6 and HA-ML@ES^{Ce6} NPs (Ce6: 5 mg.kg⁻¹). Fluorescence intensity was then measured in serum collected at different time points using an IVIS (Lumina XR). In addition, Model group mice were intravenously injected with Ce6, ML@ES NPs^{Ce6} and HA-ML@ES^{Ce6} NPs (Ce6: 5 mg.kg⁻¹) after 10 weeks of a high methionine diet (HMD). After 12 h, the aorta and other organs of the mice were analyzed using IVIS.

In vivo anti-atherosclerosis study

Six-week-old male ApoE^{-/-} mice received High Methionine Diet (HMD) consisting of 55.5% carbohydrates, 20% protein, 1.7% methionine, and 4.5% fat, and for a period of 4 weeks. Thereafter, the mice were treated to saline, Evol + SKN (2.5 mg.kg⁻¹+1.2 mg.kg⁻¹) combination

or HA-ML@ES NPs (Evol: 2.5 mg·kg⁻¹ and SKN: 1.2 mg·kg⁻¹) for a period of 8 weeks while maintaining the HMD diet. The animal experiment was approved by the Ningxia Medical University Animal Care and Use Committee (ethics approval number: 2023-G225), and the guidelines of the Ningxia Medical University Animal Care Committee were strictly followed.

After the treatment was completed, the thickness of the intima-media in the aortic root of normal, model, and HA-ML@ES NPs mice was examined using ultrasound equipment, and the blood flow velocity in the aortic root was measured. Euthanize all mice and isolate the aorta. Photographs of the aortic arch were taken. In addition, the entire aorta was fixed with 4% paraformaldehyde for 24 h. Subsequently, excess fatty tissue was removed from the aorta and the aorta was stained with 3% ORO and observed for plaque area. Cross section of aortic root stained with 3% ORO. Plaque area was quantified using ImageJ software. In addition, H&E staining was performed to assess the area of the necrotic core and Masson staining was performed to evaluate the collagen content.

Serum levels of IL-1 β , IL-6, TNF- α , and IL-10 were measured in mice using Elisa kit instructions (Quanti-Cyto, EMC001b, EMC004, EMC102a, EMC005). Immunofluorescence staining was performed against primary antibodies against CD80 and CD206 and confocal photography was performed to observe changes in M1/M2 type macrophages. Aortic valve sections were stained using an apoptosis detection kit (SEVEN, SC224-02), followed by immunofluorescence staining for CD31 (AF6191, 1:300, Affinity), and confocal photography to observe endothelial cell apoptosis. In addition, immunohistochemical staining of aortic root sections was performed using primary antibodies against the anti-apoptotic proteins Bcl-2 (68103-1-IG, 1:1000, Proteintech) and ICAM-1 (10831-1-AP, 1:300, Proteintech). Finally, the sections were subjected to immunofluorescence staining with VE-cad primary antibody. Immunofluorescence staining of aortic root sections was performed with F4/80 (Santa Cruz, USA, 1:500) antibody. In addition, paraffin-embedded aortic root sections were immunohistochemically stained using primary antibodies against the lipoprotein uptake receptor protein LOX-1 (11837-1-AP, 1:300, Proteintech) and the cholesterol transporter protein ABCG1 (13578-1-AP, 1:300, Proteintech) and photographed for imaging using an inverted microscope.

Safety evaluation

Upon completion of the treatment regimen, the mice were euthanized and blood samples were collected from each group for routine blood analysis and biochemical analysis. Simultaneously, major organs, such as the heart,

lungs, liver, spleen, and kidneys, were harvested from the mice and subjected to H&E staining for histological analysis.

Data analysis

Statistical analysis version 9.0.0 was performed using GraphPad Prism and t-test and one-way analysis of variance (ANOVA) were used to calculate the significance of the data. All results are expressed as mean \pm standard deviation and are from independent experiments.

Results and discussion

SKN inhibits apoptosis of HUVECs and evol inhibits macrophages lipid influx

Although many evidences have demonstrated that endothelial cells apoptosis and macrophage-like foam cells formation are key risk factors for the onset and progress of atherosclerosis [17, 18], the interactions of concrete proteins in these cells are not clear. In this study, we screened targets related to endothelial cells apoptosis and macrophages lipid metabolism using the Toxicogenomics Database (CTD). Then, the mined potential targets were imported into the STRING database to construct protein-protein interaction network. Figure 1A revealed the important role of apoptosis -related proteins (Bcl-2 and BAX) and lipid metabolism-related proteins (LOX-1, ABCA1 and ABCG1) in the development of AS. Next, we investigated the ability of SKN to inhibit endothelial cell apoptosis and Evol to inhibit lipid influx. At first, we investigated the effect of SKN and Evol on the cell viability of HUVECs and RAW264.7 cells. MTT assay indicated the viabilities of the two kinds of cell line were higher than 97% even at the presence of 500 nM SKN and 2.5 nM Evol (Fig. 1B&C). Then, we investigated the effect of SKN on the HUVECs apoptosis. TUNEL assay indicated that Hcy treatment induced cell apoptosis was inhibited by SKN (250 nM and 500 nM) (Fig. 1D). Flow cytometry assay showed that the rate of endothelial cell apoptosis decreased by 5.23% after SKN (250 nM) treatment compared to Hcy (Fig. 1E). Meanwhile, we investigated the effect of Evol on Dil-oxLDL uptake by RAW264.7. Fluorescence images indicated strong red fluorescence in the Hcy treated RAW264.7 cells (Hcy group). However, fluorescence signal gradually decreased in a Evol concentration-dependent manner in the range from 0.6 to 2.5 nM (Fig. 1F). Similarly, Oil Red O (ORO)-staining indicated strong red lipid droplets in Hcy treated RAW264.7 cells (Hcy group) incubating with oxLDL for 24 h. However, the presence of 1.25 nM Evol effectively reduced the signal which reflected the inhibition of oxLDL internalization in Hcy treated cells (Fig. 1G). In conclusion, the combination of 250 nM SKN and 1.25 nM Evol demonstrated an effective ability to inhibit endothelial cell apoptosis and macrophage lipid influx.

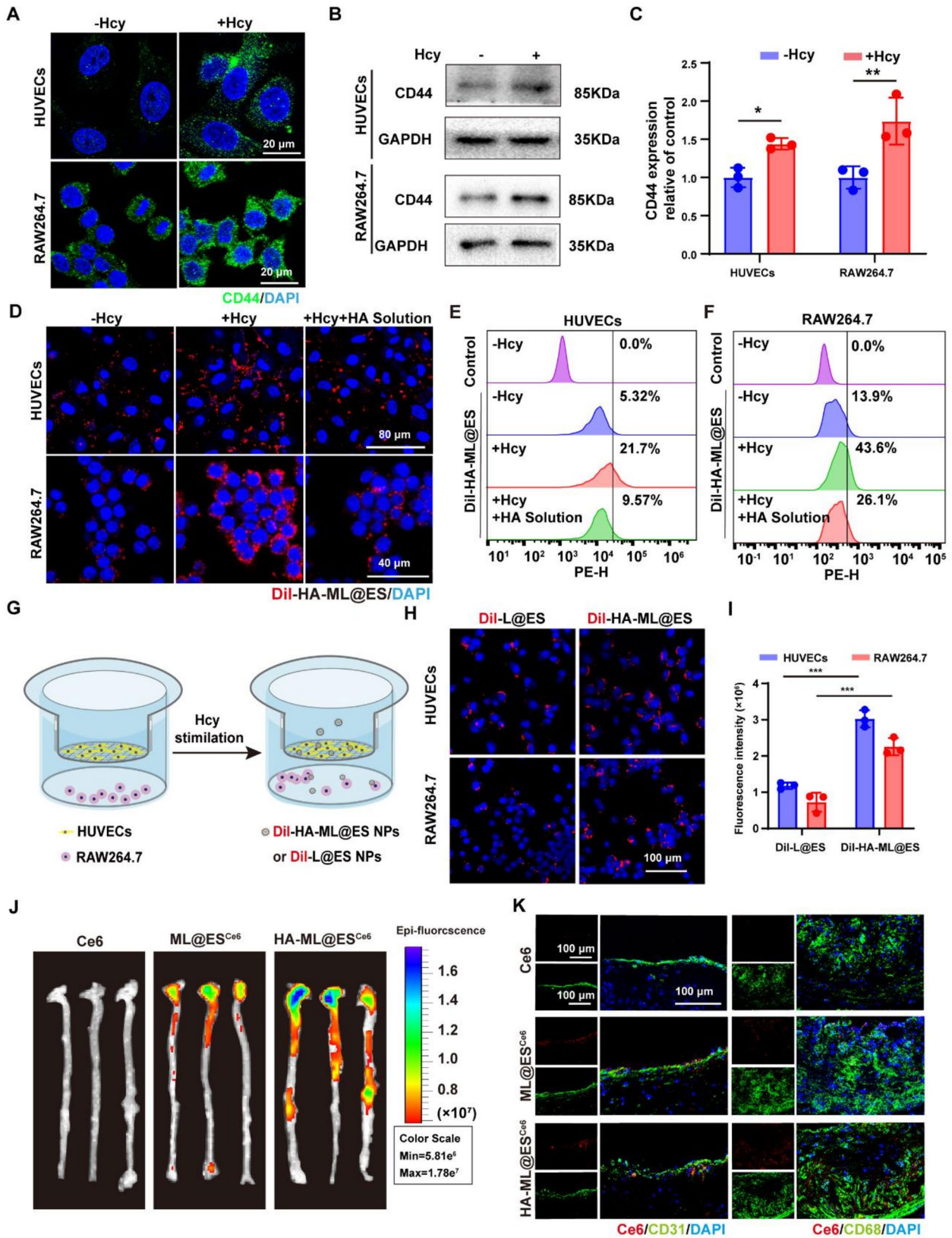


Fig. 3 (See legend on next page.)

(See figure on previous page.)

Fig. 3 Intracellular uptake and targeting ability in vivo of HA-ML@ES NPs. **(A)** Fluorescence images of CD44 in HUVECs and RAW264.7 after different treatments. [Hcy] = 100 μ M. **(B)** Western blot analysis of CD44 on HUVECs and RAW264.7 after different treatment with **(C)** quantitative data at right. [Hcy] = 100 μ M. **(D)** Representative images of CLSM of HUVECs and RAW264.7 after 4 h of incubation with Dil-HA-ML NPs. [Hcy] = 100 μ M. Scale bar = 50 μ m. **(E)** Flow cytometry analysis of HUVECs and **(F)** RAW264.7 after 4 h of incubation with PBS or Dil-HA-ML NPs. [Hcy] = 100 μ M. **(G)** Schematic diagram of the co-culture pattern of HUVECs with RAW264.7 cells. **(H)** Confocal microscopy images and **(I)** fluorescence intensity of Dil-L@ES NPs and Dil-HA-ML NPs in HUVECs and RAW264.7 cells in a trans-well system. [Hcy] = 100 μ M. Scale bar = 100 μ m. **(J)** Ex vivo fluorescence images of Ce6 fluorescence in aortas 12 h after Ce6, ML@ES^{Ce6} and HA-ML@ES^{Ce6} NPs injection into ApoE^{-/-} atherosclerotic mice. **(K)** CLSM analysis of the co-location of Ce6, ML@ES^{Ce6} NPs and HA-ML@ES^{Ce6} NPs (red) and endothelial cells (green), or Ce6, ML@ES^{Ce6} NPs and HA-ML@ES^{Ce6} NPs (red) and macrophages (green) in atherosclerotic plaques ($n = 3$) Data are mean \pm SD ($n = 3$) * $P < 0.05$, ** $P < 0.01$, **** $P < 0.001$

Fabrication and characterization of HA-ML@ES NPs

Then, using the reverse evaporation method [14], liposomes were synthesized for loading Evol and SKN (Fig. 2A). Evol and SKN were loaded in the hydrophilic chamber layer and hydrophobic layer, respectively. Then, M ϕ m was fused with L@ES NPS following with HA-PEG₂₀₀₀-DSPE modification to obtained the HA-ML@ES NPs with the Tyndall effect under laser irradiation (Fig.S1A). By optimizing the drug and lecithin ratios, it was found that the mass ratio of 20: 5: 3 for lecithin, Evol and SKN showed the highest encapsulation rate of 63.78% \pm 2.34% and 39.63% \pm 2.24%, respectively (Fig.S1B&C). TEM images indicated spherical morphology of HA-ML@ES NPs with uniform size (Fig. 2B). Then we investigated the fusion efficacy of Dil labeled liposomes and DiD labeled M ϕ m. Confocal images showed that the yellow portion of fluorescence (the overlap of red and green color), which reflected the successful fusion of M ϕ m and liposomes (Fig. 2C) The energy resonance transfer caused by membrane fusion can enhanced Dil signal [19]. The fluorescence spectra further indicated the enhancement of signals at 564 nm and weaken at 663 nm caused by the membrane fusion (Fig. 2D). In addition, SDS-PAGE assay indicated consistent protein profiles between the macrophage membrane group and the liposome membrane fusion group (Fig. 2E). Western blot analysis indicated the CD68 proteins (the marker of macrophage membrane) in the HA-ML@ES (Fig. 2F). These results strongly confirmed the successful fusion between liposome NPs and membrane. DLS assay indicated the diameter of HA-ML@ES NPs for 216.3 nm \pm 4 nm (Fig. 2G) and the potential for -18.2 mV \pm 3.7 mV, a 7.67 mV increase compared with that of ML@ES NPs due to the successful insertion of HA (Fig. 2H). Finally, we investigated the release behavior and stability of HA-ML@ES NPs. Figure 2I indicated that the cumulative release rates of SKN and Evol in HA-ML@ES NPs were 32.26% \pm 2.87% and 34.78% \pm 1.79%, respectively, over 72 h, whereas the cumulative release rates of SKN and Evol in L@ES NPs were 52.43% \pm 2.01% and 55.25% \pm 2.56%. This result demonstrated that the M ϕ m and HA-PEG₂₀₀₀-DSPE modifications can improve the stability of liposomes, which can facilitate the achievement of controlled drug release from the disease site [20]. The unchanged particle size of the synthesized HA-ML@ES NPs in

different solvents (PBS and 10% FBS) indicated the good stability (Fig. 2J).

Immune escape, targeting ability and intracellular uptake of HA-ML@ES NPs

Macrophages, an important component of the innate immune system, can rapidly clear sole drugs [21]. However, nanoformulation of drug can often attenuate the phagocytosis efficacy of macrophages [22]. Using Dil to label L@ES NPS, ML@ES NPs, and HA-ML@ES NPs, we investigated the uptake efficacy of normal macrophages to these materials through fluorescence imaging. As shown in Fig. S2A&B, the red fluorescent signals in macrophages in the Dil-ML@ES NPs group and the Dil-HA-ML@ES NPs group were significantly lower than that of Dil-L@ES NPs group. This result demonstrated that Dil-HA-ML@ES NPs can effectively reduce phagocytosis of macrophages due to the immune escape capability of M ϕ m [23].

CD44, a receptor for HA highly expressed in the inflammatory tissues, has been widely used as the target of nanodrugs with HA [24]. In this study, we investigated the effect of Hcy on the CD44 levels in HUVECs and RAW264.7 cells. Both of fluorescence imaging and western blot indicated the upregulation of CD44 caused by Hcy (green fluorescence) in HUVECs and RAW264.7 cells (Fig. 3A–C). Accordingly, CLSM analysis showed that strong green fluorescence was observed in HUVECs and RAW264.7 cells with Hcy treatment. However, the accumulation of Dil-HA-ML@ES NPs in HUVECs and RAW264.7 was drastically reduced after with excess HA pre-blockade (Fig. 3D). This result further consolidates the targeting ability of HA-ML@ES NPs through the interaction between HA and CD44. Flow cytometric analysis indicated 4.15-fold and 3.16-fold enhancement of intracellular Dil signaling in HUVECS and RAW264.7 cells in the model (+Hcy) group, compared with the normal (-Hcy) group. In contrast, the intracellular Dil signals in the HA-treated group were decreased by 56% and 39%, respectively (Fig. 3E&F). These results strongly support that HA modification confers the targeting ability of HA-ML@ES NPs to inflammatory endothelial cells and macrophages.

Next, the transwell system was adopted to assess the uptake efficacy of endothelial cells and macrophages to

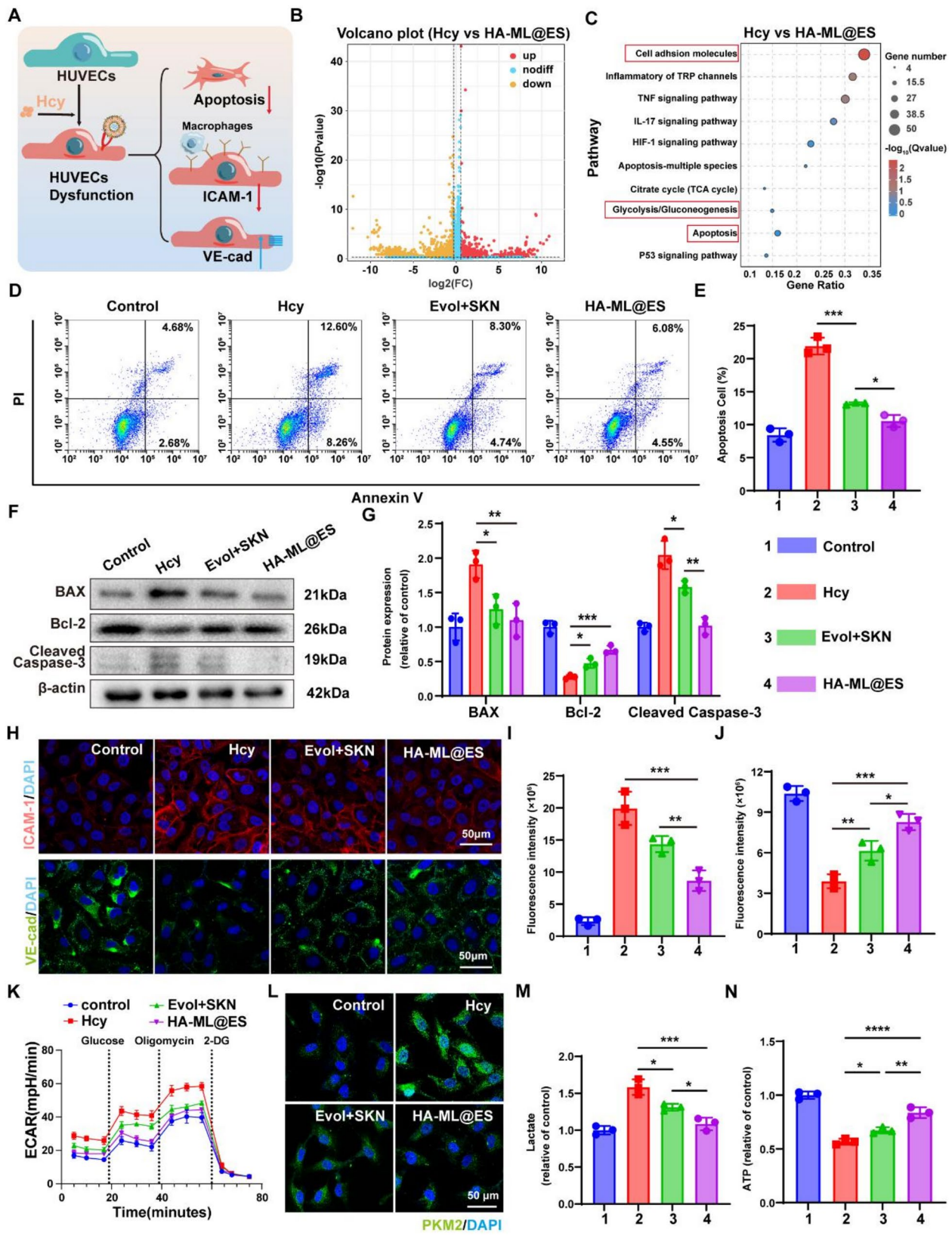


Fig. 4 (See legend on next page.)

(See figure on previous page.)

Fig. 4 HA-ML@ES NPs can restore HUVECs function. **(A)** HA-ML@ES NPs repair HUVECs pattern diagram. **(B)** Volcano plots of differentially expressed genes distribution in HUVECs treated with Hcy and HA-ML@ES NPs. [Hcy] = 100 μ M. **(C)** KEGG analysis of upregulated and downregulated cellular pathways in HUVECs caused by HA-ML@ES NPs. **(D)** Flow cytometry analysis and **(E)** quantitative analysis of HUVECs apoptosis. [Hcy] = 100 μ M. **(F)** Western blot assay and **(G)** quantitative analysis of BAX, Bcl-2, and Cleaved caspase-3 levels in HUVECs with different treatments. [Hcy] = 100 μ M. **(H)** CLSM images of ICAM-1 and VE-cad on HUVECs with different treatment. [Hcy] = 100 μ M. Scale bar = 50 μ m. **(I)** Quantitative analysis of ICAM-1 staining. **(J)** Quantitative analysis of ICAM-1 staining. **(K)** ECAR profile showing glycolytic function of glycolytic function parameters in HUVECs under different treatment. [Hcy] = 100 μ M. Vertical lines indicate the time of addition of glucose (10 mM), oligomycin (1 μ M), and 2-DG (50 mM) (n = 3). **(L)** CLSM images of PKM2 in HUVECs with different treatment. Scale bar = 50 μ m. **(M&N)** Measurement of L-lactic acid APT content in HUVECs. Data are mean \pm SD (n = 3) * P < 0.05, ** P < 0.01, *** P < 0.001, **** P < 0.0001

HA-ML@ES NPs. Hcy-treated HUVECs and RAW264.7 cells were cultured in the upper and lower chambers, respectively, to simulate the plaque (Fig. 3G). Fluorescence imaging indicated the significantly stronger red fluorescence in HUVECs and RAW264.7 cells with Dil-HA-ML@ES NPs incubation, compared to that of Dil-L@ES NPs (Fig. 3H&I). These findings further confirmed the importance of HA modification for improving the internalization efficiency of HA-ML@ES NPs by HUVECs and macrophages.

Encouraged by the in vitro results, then, we investigated the circulating half-life using male Kunming mouse as the model as previously reported [25]. After injection of Ce6 and HA-ML@ES^{Ce6} NPs via the tail vein, we measured the fluorescence signal intensity of Ce6 and HA-ML@ES^{Ce6} NPs in blood samples. Fig. S3A&B indicated the longer half-life time of HA-ML@ES^{Ce6} NPs relative to sole Ce6 ($t_{1/2}$ = 1.31 h VS $t_{1/2}$ = 0.52 h), These results strongly support that M ϕ m prolongs the circulation time of HA-ML@ES NPs, which facilitates SKN and Evol accumulation in atherosclerotic plaques [26]. Moreover, we evaluated the biodistribution of Ce6 and HA-ML@ES^{Ce6} NPs in AS mice using an in vivo imaging system (IVIS). Figure 3J&S4 indicated that the fluorescence signal intensity of ML@ES^{Ce6} NPs at the aortic site was enhanced by 1.8-fold, compared with that of Ce6, which was attributed to the “homing effect” of NPs increased by the modification of M ϕ m [27]. More importantly, the fluorescence signal intensity of HA-ML@ES^{Ce6} NPs at the aortic site was enhanced by 1.5-fold, compared with that of ML@ES^{Ce6} NPs, which result demonstrated the atherosclerotic plaques targeting ability of HA-ML@ES^{Ce6} NPs through the interaction of HA with highly expressed CD44 expression on the surface of damaged endothelial cells and inflammatory macrophages [28]. Meanwhile the accumulation of ML@ES^{Ce6} NPs and HA-ML@ES^{Ce6} NPs were found to be higher in the liver compared to Ce6 alone, probably because M ϕ m modification prolonged Ce6 blood circulation time, and the content of HA-ML@ES^{Ce6} NPs in mice was higher than that of the Ce6 group after 12 h. In addition, our findings showed robust signaling distribution in hypermetabolic tissues (e.g. liver and kidney) (Fig. S5A&B).

Furthermore, immunofluorescence staining with the endothelial cell marker CD31 and the macrophage

marker CD68 was adopted to investigate the intracellular distribution of Ce6, ML@ES^{Ce6} NPs and HA-ML@ES^{Ce6} NPs in the aortic root sections. Figure 3K indicated the co-localization of HA-ML@ES^{Ce6} NPS with CD31⁺ endothelial cells and CD68⁺ macrophages, underscoring the dual targeting proficiency of both cell types that are pathologically relevant to AS. Collectively, these findings underscore the efficacy of HA-ML@ES NPs for selectively targeting endothelial cells and macrophages in the context of AS. In addition, it has been shown that both macrophages and T cells play important roles in the development of atherosclerosis, with a high percentage of macrophages (28.9%) and T cells (19.6%) among immune cells at the plaque site and high expression of CD44 on the surfaces of both macrophages and T cells [29, 30]. We also performed immunofluorescent staining with the T-cell marker CD3 to study the intracellular distribution of Ce6, ML@ES^{Ce6} NPs and HA-ML@ES^{Ce6} NPs in aortic root sections. Fig. S6 showed that there was a weak localization between HA-ML@ES^{Ce6} NPS and CD3⁺ T cells. These results indicated that HA-ML@ES NPs may can inhibit AS by regulating immune microenvironment.

HA-ML@ES NPs can efficiently restore HUVECs function by inhibiting apoptosis

Previous studies have shown that Hcy can induce apoptosis and upregulate intercellular adhesion molecules to impair endothelial barrier, which finally result in the onset and progression of atherosclerosis [31–33]. Using Hcy treated HUVECs as model, we adopted RNA sequencing assay to investigate the effect of HA-ML@ES NPs on the gene transcription (Fig. 4A). Principal component analysis showed significant differences among the three groups of Control, Model, and HA-ML@ES NPs (Fig. S7A). A total of 1580 differentially expressed genes were identified between Control and Hcy, including up-regulated 886 genes and down-regulated 694 genes in Hcy group. (Fig. S7B), while 1796 differentially expressed genes were identified between Hcy and HA-ML@ES NPs, of which 736 were up-regulated and 1060 were down-regulated in HA-ML@ES NPs group (Fig. 4B). Venn plots showed a total of 776 genes intersected in the three groups (Fig. S7C). Notably, KEGG analysis indicated that up-regulate genes involved in cell adhesion molecule pathway, apoptotic pathway, and glycolytic pathway in the model

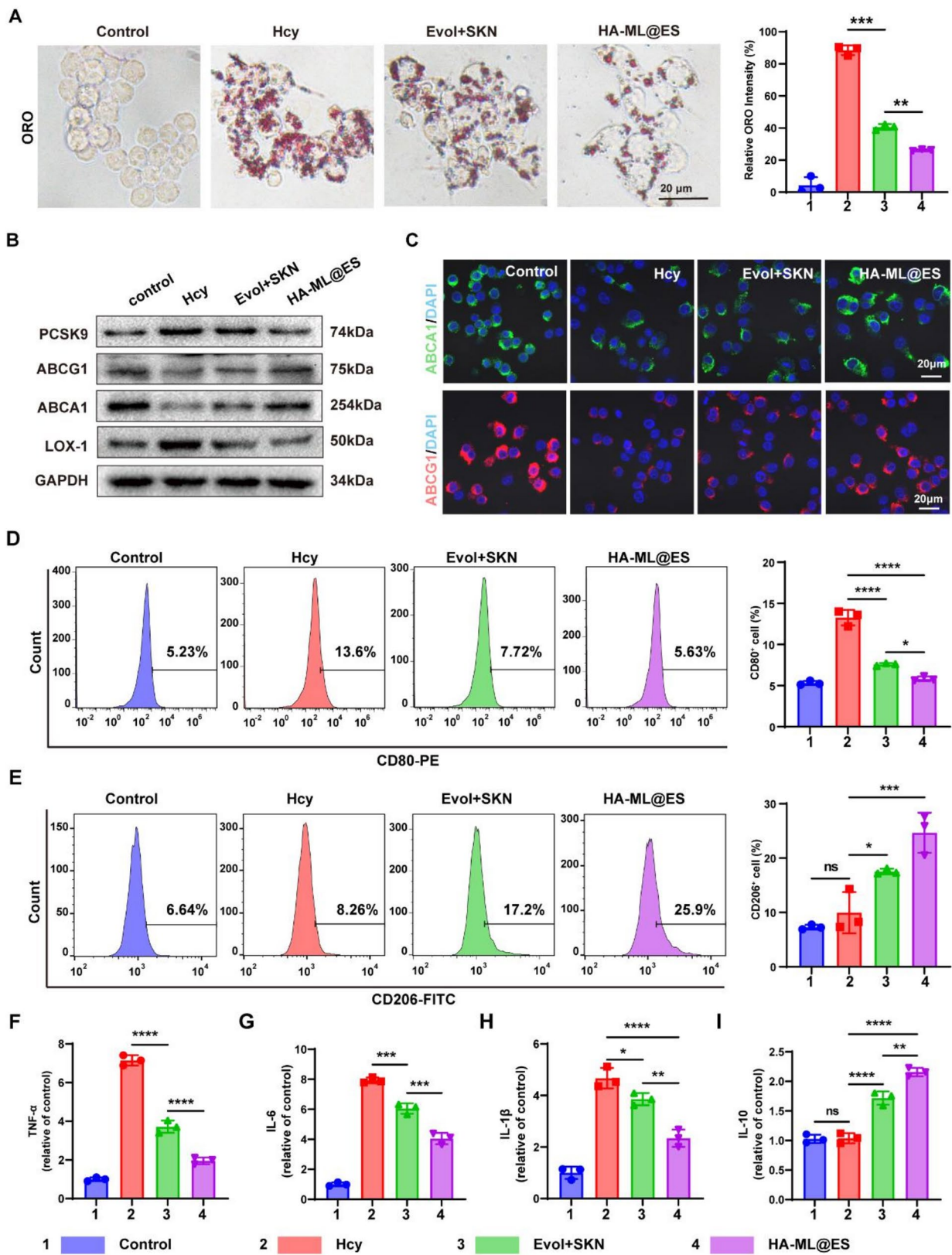


Fig. 5 (See legend on next page.)

(See figure on previous page.)

Fig. 5 HA-ML@ES NPs modulate macrophage polarization to restore cholesterol flow homeostasis in vitro. **(A)** Optical microscopy images of oxLDL internalization in Hcy induced RAW264.7 cells. [Hcy]= 100 μ M, [ox-LDL]= 80 μ g/mL. Scale bar = 20 μ m. **(B)** Western blot analysis of PCSK9, ABCA1/G1 and LOX-1 on macrophages with different treatment. [Hcy]= 100 μ M. **(C)** CLSM images of ABCA1/G1 on RAW264.7 cells with different treatment. Scale bar = 20 μ m. [Hcy]= 100 μ M. **(D)** Flow cytometry results of macrophage polarization after treatment with different nanoparticles and **(E)** quantitative data at right. [Hcy]= 100 μ M. **(F-I)** ELISA detected typical inflammatory cytokines TNF- α , IL-6, IL-1 β and IL-10 secreted by Hcy treated RAW264.7 cells. [Hcy]= 100 μ M. Data are mean \pm SD ($n=3$) * $P<0.05$, ** $P<0.01$, *** $P<0.001$, **** $P<0.0001$

group were reversed by the HA-ML@ES NPs treatment (Fig. 4C, S7D&E). Flow cytometry assay indicated the early and late apoptosis rates in the model group were 8.26% and 12.60% in HUVECs, respectively. However, the corresponded apoptosis rates were 3.71% and 6.52% in the HA-ML@ES NPs-treated group (Fig. 4D&E). Western blot indicated that the level of apoptosis-related Bcl-2 was up-regulated by 2.4-fold, while the level of BAX was down-regulated by 42% in HA-ML@ES NPs treated cells, compared to the model group. Moreover, 51% decrease of Cleaved caspase-3 was observed in the same group (Fig. 4F&G). Overall, these results clearly confirmed that HA-ML@ES NPs inhibited apoptosis in HUVECs. Meanwhile, Fluorescence imaging indicated that red signal, which represents the levels of ICAM-1, a molecule for recruiting macrophages to promote AS [34], (red fluorescence) significantly downregulated in HA-ML@ES NPs treated inflammatory HUVECS (Fig. 4H&I), along with a significant decrease in VE-cadherin (VE-cad) (green fluorescence) (Fig. 4H&J), an endothelium-specific adhesion molecule for maintaining endothelial cell integrity and preventing AS.

It was reported that Hcy can increase aerobic glycolysis by upregulating the activity of PKM2, the rate-limiting enzyme in aerobic glycolysis, which ultimately leads to the accumulation of lactate, the end product of glycolysis [35]. Whereas elevated glycolysis may trigger activation of inflammatory pathways causing apoptosis [36, 37]. SKN, as a PKM2 inhibitor, is expected to improve endothelial cell energy metabolism and inhibit endothelial cell apoptosis by inhibiting PKM2 [38]. At first, we assessed the glycolytic metabolism of HUVECs treated with HA-ML@ES NPs by measuring extracellular acidification rate (ECAR) by Seahorse extracellular flux analysis. As shown in Fig. 4K& S8, HA-ML@ES NPs reduced the elevated basal ECAR (from 28.9 ± 2.4 to 18.3 ± 2.1 mpH/min) while suppressing the Hcy-induced maximal ECAR elevation (from 57.3 ± 3.7 to 44.4 ± 1.1 mpH/min), reflecting a HA-ML@ES NPs-induced maximal glycolytic potential decreased. Further studies revealed that HA-ML@ES NPs significantly inhibited activity of PKM2 (green fluorescence), accordingly reduced the accumulation of lactate (Fig. 4L&M). In contrary, the levels of ATP, a key energy molecule decreased in apoptosis cells [39], significantly increased in cells with HA-ML@ES NPs treatment (Fig. 4N). These results demonstrated

that HA-ML@ES NPs can HUVECs inhibit apoptosis by improving energy metabolism.

HA-ML@ES NPs can reprogram macrophage polarization in vitro

The accumulation of inflammatory macrophages with exceed oxLDL internalization in the intima is a significant characteristic of atherosclerotic lesions, playing a crucial role in the progression of AS [40]. Moreover, these macrophages can activate PCSK9 expression, increase the oxLDL uptake receptor protein LOX-1, while inhibit cholesterol transporter proteins ABCA1 and ABCG1, which finally lead to foam cell formation [41, 42]. Thus, restoring the balance of cholesterol flow within plaque is urgent for inhibiting atherosclerosis progression. By using ORO staining to investigating the effect of HA-ML@ES NPs on the lipid internalization it was found the significant reduction of intracellular lipid droplets in the Hcy treated macrophages after treatment with HA-ML@ES NPs (Fig. 5A). Accordingly, western blot indicated that HA-ML@ES NPs downregulated PCSK9 and LOX-1, while upregulated ABCA1/ABCG1 in the Hcy treated macrophages (Fig. 5B). Confocal microscopy images visually showed the significant upregulation of ABCA1 and ABCG1 caused by HA-ML@ES NPs (Fig. 5C). Flow cytometry assay indicated that the ratio of M1/M2 was significantly decreased in Hcy-treated macrophages after with HA-ML@ES NPs treatment, which is lower than that of sole Evol+SKN treatment (Fig. 5D&E). Accordingly, the decrease of pro-inflammatory cytokines TNF- α , IL-6 and IL-1 β and significant increase of anti-inflammatory cytokine IL-10 was found in Hcy-treated macrophages with HA-ML@ES NPs treatment (Fig. 5F-I). These results suggested that HA-ML@ES NPs can reverse M1 macrophage polarization to abrogate inflammation and inhibit foaming cell formation, which is beneficial for ultimately restoring cholesterol flow homeostasis and intervening the development of atherosclerosis.

HA-ML@ES NPs effectively treat early atherosclerosis

Based on these promising findings, we validate the therapeutic potential of HA-ML@ES NPs in Hcy-induced ApoE^{-/-} AS mice (Fig. 6A). The mice were given 4 weeks of the HMD diet to produce early atherosclerotic plaques, and maintain the diet plus Evol+SKN or HA-ML@ES NPs treatment for 8 weeks. In order to evaluate efficacy, Ultrasonography images in Fig. S9A-C indicated

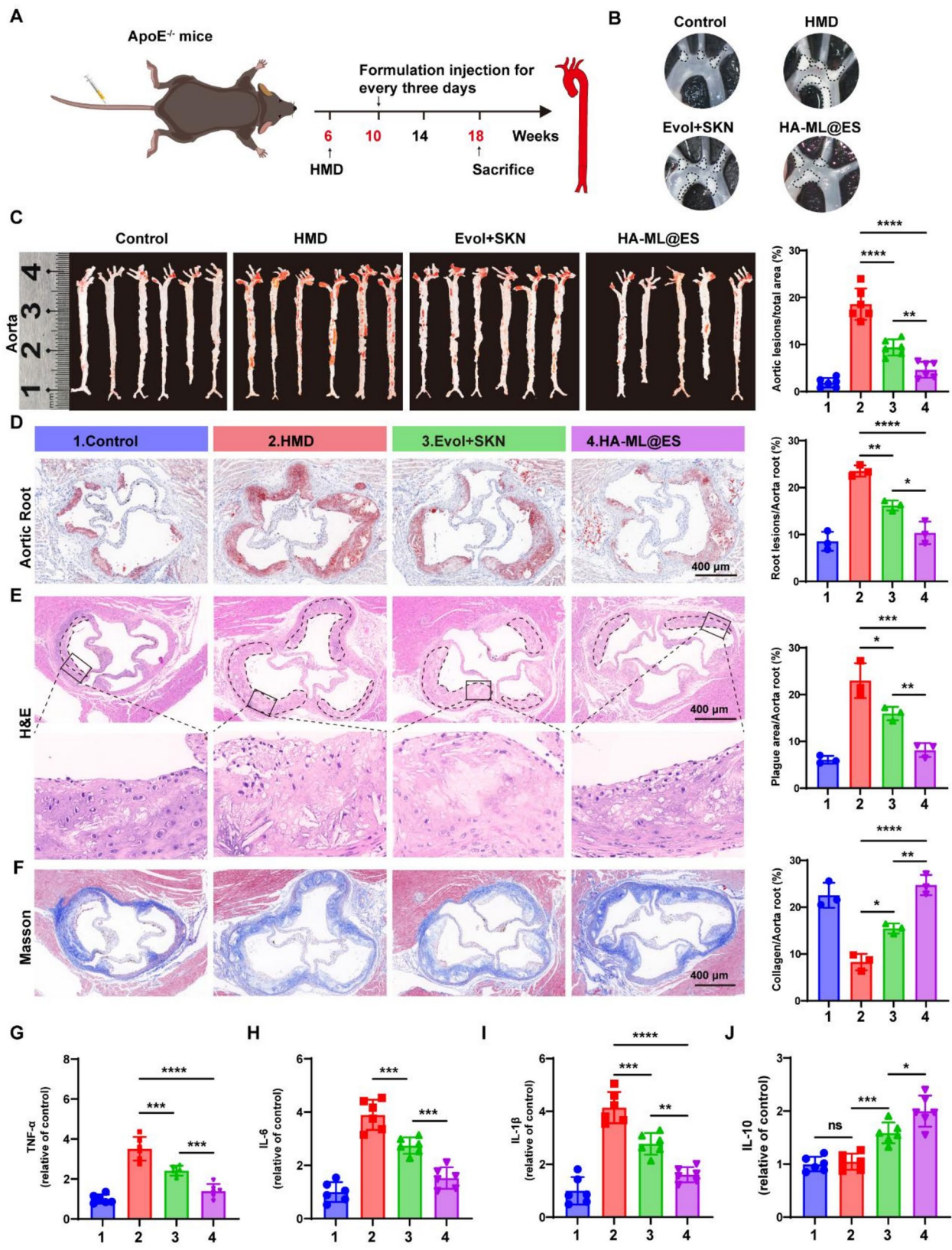


Fig. 6 (See legend on next page.)

(See figure on previous page.)

Fig. 6 HA-ML@ES NPS effectively treat early atherosclerosis. **(A)** A schematic diagram illustrating the in vivo treatment mode. **(B)** Photographs of the aortic arch ($n=6$). **(C)** Quantitative analysis of aortic surface ORO staining images and lesion sites ($n=6$). **(D)** ORO staining of aortic roots and quantitative analysis of lesion sites. Scale bar = 400 μm . ($n=3$). **(E)** Representative H&E staining images and quantitative analysis of plaque area. Scale bar = 400 μm . ($n=3$). **(F)** Representative Masson staining images and quantitative analysis of plaque area. Scale bar = 400 μm ($n=3$). **(G)** ELISA detected typical inflammatory cytokines TNF- α , **(H)** IL-6, **(I)** IL-1 β and **(J)** IL-10 secreted in serum ($n=6$). Data are mean \pm SD ($n=3$) * $P < 0.05$, ** $P < 0.01$, *** $P < 0.001$, **** $P < 0.0001$

significant thickening of intima-media thickness (IMT) and increase in blood flow velocity in the aortic root of ApoE^{-/-} mice with HMD diet. However, the administration of HA-ML@ES NPs significantly decreased both IMT and blood flow velocity. The isolated aorta visually indicated significant reduction in plaque size in the aortic arch region (area circled by the black dotted line) of mice with HA-ML@ES NPs administration (Fig. 6B). ORO staining showed that the area of lipid accumulation in the plaques was approximately 1.89% and 18.58% in the control and model groups, respectively. However, the plaque areas of AS mice were approximately 9.39% and 4.62% after with Evol + SKN and HA-ML@ES NPs administration, respectively (Fig. 6C). These results demonstrated the strong inhibitory effect of HA-ML@ES NPs on the AS plaques formation. Moreover, ORO staining of aortic valves showed significant lipid accumulation within plaques in the model group, whereas the lipid accumulation was significantly reduced after HA-ML@ES NPs treatment (Fig. 6D). H&E staining also showed the least inflammatory response in the aortas of HA-ML@ES NPs-treated ApoE^{-/-} mice, as evidenced by the smallest proportion of necrotic cores in the resulting plaques. (Fig. 6E). Masson's trichromatic method showed the increase of collagen content around the plaques and the thickness of the fibrous cap of mice with HA-ML@ES NPs treatment (Fig. 6F), suggesting the improved plaque stability [37]. ELISA assay indicated that the inflammatory factor indexes, the pro-inflammatory factors TNF- α and IL-6 decreased and the anti-inflammatory factor IL-10 increased in the blood of HA-ML@SE NPs-treated mice, compared with the model group (Fig. 6G-J). Overall, the above results suggest that HA-ML@ES NPs with strong anti-inflammatory function can effectively inhibit the development of atherosclerosis and increase the stability of atherosclerotic plaques.

HA-ML@ES NPs repair endothelial cells function in ApoE^{-/-} atherosclerotic mice

It was reported that endothelial cell apoptosis played a key role in the pathogenesis of AS as enlarged cellular gaps caused by endothelial cell apoptosis lead to the entry of inflammatory macrophages into the subendothelial layer [4]. Using immunofluorescence staining on the cross-sections of the aortic root, we found that HMD diet resulted in the significant increase in CD31-labelled endothelial apoptotic cells (green fluorescence), compared to the normal diet group. However, HA-ML@

ES NPs treatment resulted in a decrease in CD31-labelled endothelial apoptotic cell (Fig. 7A&B) and significant upregulation of Bcl-2 protein at the lesion site (Fig. 7C&D). These findings confirmed the inhibitory effect of HA-ML@ES NPs on the endothelial apoptosis. In addition, it was reported that endothelial cells apoptosis can upregulate the levels for ICAM-1 during the early stage of atherosclerosis [43, 44]. In this study, using immunohistochemical staining, we found significant ICAM-1 decrease at the lesion site of aortic root of mice treated with HA-ML@ES NPs (Fig. 7E&F). Then, immunofluorescence imaging, which can illustrate the localization of VE-cad in aorta, was used to explore the effect of HA-ML@ES NPs on the endothelial barrier function. As shown in Fig. 7G&H, separate red fluorescent signal, which represents the levels of VE-cad, was found in the HMD diet (Model) group due to the endothelial cell dysfunction. However, treatment of HA-ML@ES NPs significantly improved the continuity of red fluorescent signal in endothelial cells. These findings suggest that HA-ML@ES NPs can inhibit endothelial cell apoptosis to restore endothelial cell function.

HA-ML@ES NPs restore cholesterol flow homeostasis in ApoE^{-/-} atherosclerotic mice

Dysfunctional endothelial cells caused macrophage infiltration in the vasculature is an important feature of AS plaque formation [45]. Using F4/80 (macrophage-specific marker) antibody to perform Immunofluorescence staining of aortic root sections, strong green fluorescence was found in the model group, which reflected a large macrophages infiltration. However, HA-ML@ES NPs administration significantly reduced the intensity of green fluorescence, which reflected the strong inhibitory function on the macrophage infiltration (Fig. 8A). In addition, we also investigated the effect of HA-ML@ES NPs on the macrophage phenotype in vivo. Immunofluorescence staining using CD80 (M1-like macrophage marker) antibody and CD206 (M2-like macrophages marker) antibody indicated that predominant M1-like phenotype macrophages in the model group, which was reflected by the green fluorescence (Fig. 8B&C). However, HA-ML@ES NPs administration caused significant increase for the number of M2-like macrophages, which is higher than that of Evol + SKN (Fig. 8B&D). These results emphasize the function of HA-ML@ES NPs for switching macrophages from pro-inflammatory to anti-inflammatory phenotype, which accordingly reduce the inflammation

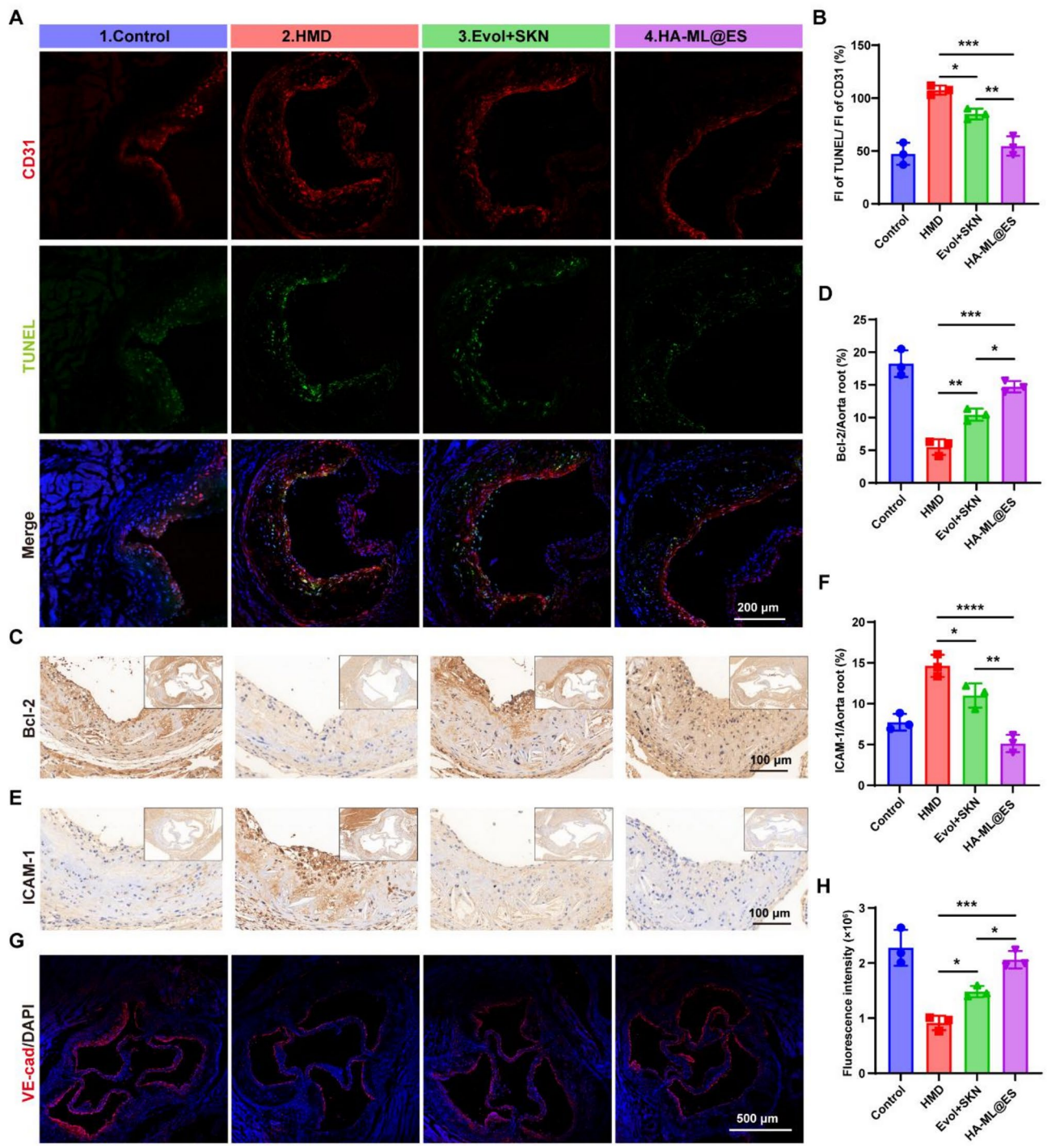


Fig. 7 HA-ML@ES NPs repairing endothelial function of ApoE^{-/-} atherosclerotic mice. **(A)** CLSM images of CD31 and TUNEL staining in aortic root sections and **(B)** quantitative analysis. Scale bar = 200 μ m. **(C-F)** Representative histochemistry images and quantitative analysis of aortic root cross-sections stained with Bcl-2 antibody and ICAM-1 antibody. Scale bar = 400 μ m. **(G)** Immunofluorescence staining images and **(H)** quantitative analysis of VE-cad in aortas Scale bar = 500 μ m. Data are mean \pm SD ($n=3$) * $P < 0.05$, ** $P < 0.01$, *** $P < 0.001$, **** $P < 0.0001$

at the plaque site. It was reported that alleviating the inflammatory microenvironment can inhibit the uptake of oxLDL mediated by LOX-1, while promote cholesterol efflux mediated ABCG1 in the plaque site [46]. Immunofluorescence staining of aortic root section showed

LOX-1 downregulation and upregulation of ABCG1 caused by HA-ML@ES NPs (Fig. 8E-G). This result suggested that HA-ML@ES NPs can restore cholesterol flow homeostasis by inhibiting LOX-1, while

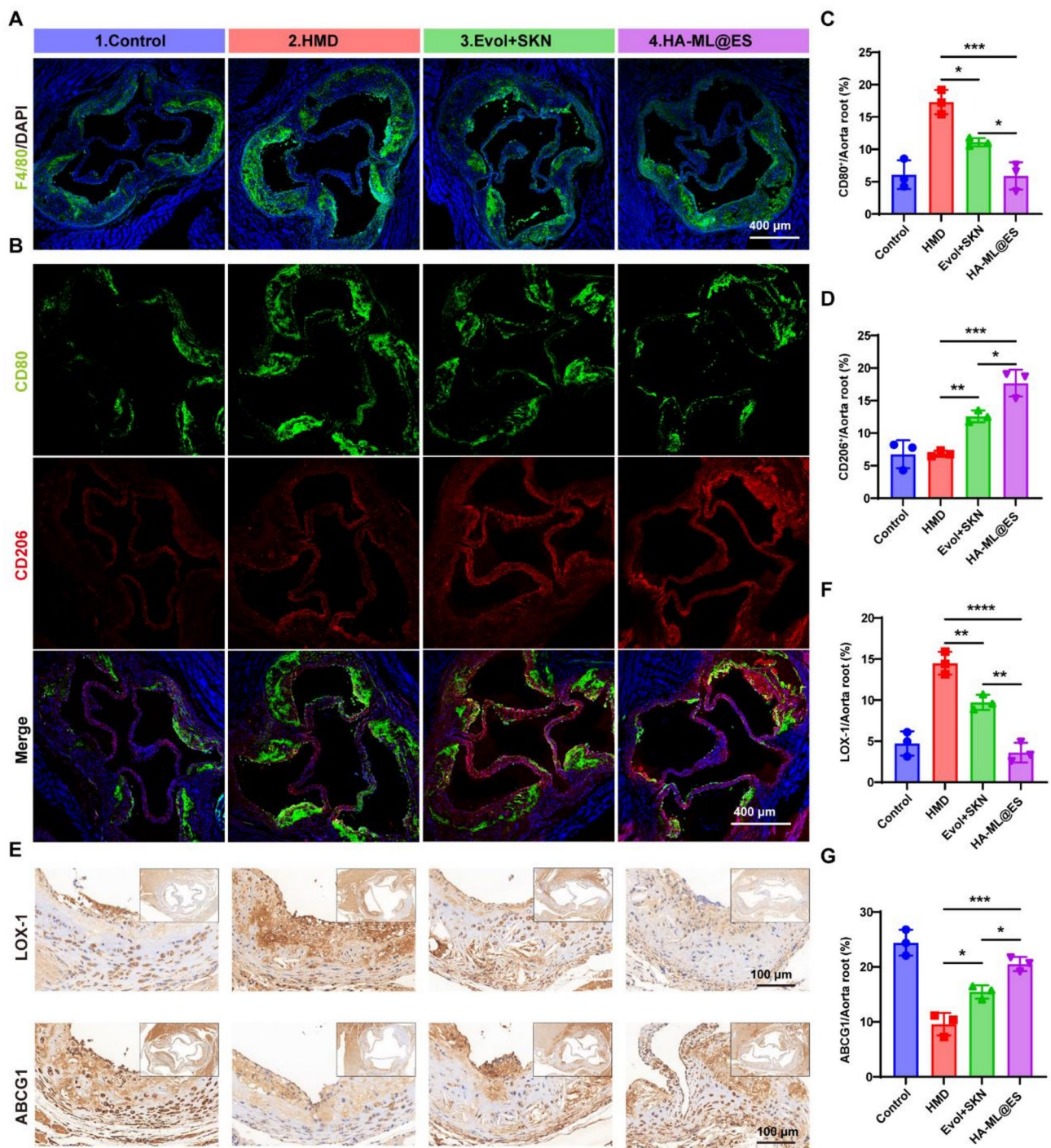


Fig. 8 HA-ML@ES NPs regulate macrophage polarization to restore cholesterol flow homeostasis. **(A)** Immunofluorescence staining images of F4/80 in aortas Scale bar = 400 μ m. **(B)** Representative images and **(C)** quantitative analysis of CD80 and **(D)** CD206 staining in aortic root sections. Scale bar = 400 μ m. **(E)** Representative histochemistry images and **(F)** quantitative analysis of aortic root cross-sections stained with LOX-1 and **(G)** ABCG1 antibody. Scale bar = 100 μ m. Data are mean \pm SD (n=3) * P < 0.05, ** P < 0.01, *** P < 0.001, **** P < 0.0001

upregulating ABCG1 expression, which finally ameliorates atherosclerosis.

Myo-inositol and glycerol mediated the restoration of cholesterol homeostasis

Moreover, metabolomics assays to investigate the regulation of HA-ML@ES NPs on the lipid metabolism. Principal component analysis showed significant differences between Control, Model and HA-ML@ES NPs (Fig. S10A&B). Volcano plots indicated a total of 279 differential metabolites between Control and Model group, while 300 differential metabolites were identified between Model and HA-ML@ES (Fig. S10C&D). Wayne diagram indicated the intersection of 222 metabolites between Model and HA-ML@ES NPs groups (Fig. S10E). Meanwhile, the KEGG analysis plot indicated significant enrichment of ABC transport pathway in the Control vs. Model group (Fig. S10F&G). Among ABC transporter pathway related specific metabolites, significant decrease of myo-inositol and increase of glycerol was found in the model group, compared to the control group. However, HA-ML@ES NPs significantly reversed the levels of myo-inositol and glycerol to the normal range (Fig. S10H). Considering the anti-atherosclerotic effect of Myo-inositol and the important raw material of glycerol for the synthesis of triglycerides, which can cause atherosclerosis [47, 48], these results demonstrate the HA-ML@ES NPs can promote the production of myo-inositol, while inhibit the production of glycerol, thus inhibit the development of atherosclerosis. However, the concrete mechanism should be deeply investigated.

In vitro and vivo biosafety

The hemocompatibility and cellular safety of nanomedicines are prerequisites for in vivo application [49]. In the hemolysis assay, the hemolysis rate of both Evol + SKN and HA-ML@ES groups was less than 5% compared to the ddH₂O-treated group (Fig. S11A) and no anomalous erythrocytes were detected from the erythrocyte morphology images (Fig. S11B). Coagulation assay indicated little effect of the Evol + SKN and HA-ML@ES groups on platelet aggregation, compared to the thrombin group (Fig. S11C), the result of which reflected a low risk of thrombosis after intravenous administration. Afterwards, Evol + SKN and HA-ML@ES NPs were co-incubated with four types of cells (HUVECs, RAW264.7, VSMC and H9C2 cells) and MTT results showed that the nanomedicine had no toxic side effects on these cells (Fig. S11D). The biosafety of the nanomaterials was further verified by co-culturing HA-ML@ES NPs with zebrafish, and no obvious abnormalities and malformations were produced from the zebrafish eggs and adult fish morphology as compared to the normal group (Fig. S11E). Afterwards, no significant difference was found for the heart rate and

body length of adult fish with HA-ML@ES NPs treatment (Fig. S11F&G). These results indicated the biosafety of this nanomaterial.

H&E staining of major organs showed no obvious traces of tissue damage or inflammatory cell infiltration in major organs such as heart, liver, spleen, lungs and kidneys in the HA-ML@ES NPs treated group (Fig. S12A). Blood counts and live and kidney function tests were also within normal limits (Fig. S12B). Moreover, LDL and CHO decreased in the HA-ML@ES NPs group, compared with the Model, which reflected the function of lowering blood lipids. These findings demonstrate the safety of HA-ML@ES NPs in the treatment of AS.

Conclusion

In conclusion, we have successfully developed a dual-targeting bio-liposomes nanodrug (HA-ML@ES NPs) capable of loading both SKN and Evol. HA-ML@ES NPs after modification with M ϕ m and HA not only prolonged the half-life of the drug but also efficiently co-delivered the drug to the damaged endothelial cells and inflammatory macrophages at the plaque site of AS. SKN and Evol play key roles in repairing endothelial cell dysfunction, inhibiting inflammatory responses and balancing cholesterol flow in macrophages, thus effectively treating early AS. Furthermore, L NPs-mediated delivery maximizes the efficacy of SKN and Evol while effectively reduced organ toxicity. Our research uses bionics and nanomedicine to provide more effective and targeted treatment options for atherosclerosis and other inflammatory diseases, advancing personalized and precision medicine.

Supplementary Information

The online version contains supplementary material available at <https://doi.org/10.1186/s12951-025-03436-5>.

Supplementary Material 1

Acknowledgements

This work was supported by Noncommunicable Chronic Diseases-National Science and Technology Major Project (Nos.2024ZD0531200); The National Natural Science Foundation of China (Nos. U21A20343); Key Projects of the Key R&D Program of the Ning Xia Hui Autonomous Region (Nos. 2023BEG02074, 2022BFH02013, 2022BEG02054); The Natural Science Foundation of Ningxia Hui Autonomous Region (Nos. 2023AAC005035); Open Competition Mechanism to Select the Best Candidates for Key Research Projects of Ningxia Medical University (Nos. XJKF240301, XJKF240304, XJKF230125 and XJKF240326). The authors thank the School of Biology, Hunan University for the help on technology and instrumentation.

Author contributions

Q.Z.: Data curation, Formal analysis, Writing—original draft. S.C.Ma.: Data curation, Investigation. X.K.: Formal analysis, Data curation. Y.L. and Fei Ma.: Data curation, Validation. F.F.Y. and X.L.L.: Investigation, Methodology. G.Z. L. and Y.J. H.: Conceptualization, Resources. H.P. Z., B. L. and Y.D. J.: Conceptualization, Methodology, Funding acquisition, Supervision, Writing—review & editing. All authors read and approved the final manuscript.

Data availability

Data is provided within the manuscript or supplementary information files.

Declarations

Ethics approval and consent to participate

The animal experiment was approved by the Ningxia Medical University Animal Care and Use Committee (ethics approval number: 2023-G225), and the guidelines of the Ningxia Medical University Animal Care Committee were strictly followed.

Consent for publication

Written informed consent was obtained from all participants.

Competing interests

The authors declare no competing interests.

Received: 15 January 2025 / Accepted: 1 May 2025

Published online: 20 May 2025

References

1. Armitage J. The safety of Statins in clinical practice. *Lancet*. 2007;370(9601):1781–90.
2. Björkegren JLM, Lusis AJ. Atherosclerosis: recent developments. *Cell*. 2022;185(10):1630–45.
3. Tamargo IA, Baek KI, Kim Y, Park C, Jo H. Flow-induced reprogramming of endothelial cells in atherosclerosis. *Nat Rev Cardiol*. 2023;20(11):738–53.
4. Ma L, Wang X, Xiang P, Chen Q, Zhao Y, Hassan M, Yu C. N-Acetylneuraminic acid induces vascular endothelial dysfunction through targeting Muc/SQSTM1 pathway and attenuates atherosclerosis. *Blood*. 2023;142(Supplement 1):1205–1205.
5. Adkar SS, Leeper NJ. Efferocytosis in atherosclerosis. *Nat Rev Cardiol*. 2024;21:762–79.
6. Shirai T, Nazarewicz RR, Wallis BB, Yanes RE, Watanabe R, Hilhorst M, Tian L, Harrison DG, Giacomini JC, Assimes TL, Goronzy JJ, Weyand CM. The glycolytic enzyme PKM2 bridges metabolic and inflammatory dysfunction in coronary artery disease. *J Exp Med*. 2016;213(3):337–54.
7. Huang CS, Lin AH, Yang TC, Liu KL, Chen HW, Lii CK. Shikonin inhibits oxidized LDL-induced monocyte adhesion by suppressing NFκB activation via up-regulation of PI3K/Akt/Nrf2-dependent antioxidant in EA.hy926 endothelial cells. *Biochem Pharmacol*. 2015;93(3):352–61.
8. Koren MJ, Descamps O, Hata Y, Hengeveld EM, Hovingh GK, Ikonomidis I, Radu Juul Jensen MD, Langbakke IH, Martens F, Søndergaard AL, Witkowski A, Koenig W. PCSK9 Inhibition with orally administered NNC0385-0434 in hypercholesterolemia: a randomised, double-blind, placebo-controlled and active-controlled phase 2 trial. *Lancet Diabetes Endocrinol*. 2024;12(3):174–83.
9. Cheeley MK, Saseen JJ, Agarwala A, Ravilla S, Ciffone N, Jacobson TA, Dixon DL, Maki KC. NLA scientific statement on Statin intolerance: a new definition and key considerations for ASCVD risk reduction in the Statin intolerant patient. *J Clin Lipidol*. 2022;16(4):361–75.
10. Rifai MA, Ballantyne CM. PCSK9-targeted therapies: present and future approaches. *Nat Rev Cardiol*. 2021;18(12):805–6.
11. Cern A, Marcus D, Tropsha A, Barenholz Y, Goldblum A. New drug candidates for liposomal delivery identified by computer modeling of liposomes' remote loading and leakage. *J Control Release*. 2017;252:18–27.
12. Xu J, Yan N, Wang C, Gao C, Han X, Yang C, Xu J, Wang K, Mitchell MJ, Zhang Y, Nie G. Platelet-Mimicking nanospheres for functional reversal of antiplatelet agents. *Circ Res*. 2023;132(3):339–54.
13. Li YL, Yang AN, Sun Y, Liu DY, You PD, Zeng YL, Quan SK, Zhang HW, Zhang HP, Ma SC, Hao YJ, Xiong JT, Liu B, Li GZ, Jiang YD. Hydroxysafflor yellow A-loaded biomimetic liposomes alleviate Hcy-induced atherosclerosis by regulating methylation related autophagy. *Mater Design*. 2023;227:111807.
14. Li Z, Zhu H, Liu H, Liu D, Liu J, Jiang J, Zhang Y, Qin Z, Xu Y, Peng Y, Liu B, Long Y. Evolocumab loaded Bio-Liposomes for efficient atherosclerosis therapy. *J Nanobiotechnol*. 2023;21(1):158.
15. Xu M, Zhou Y, Ren C, Liang X, Li N. Palladium hydride nanopocket cubes and their H₂-Therapy function in amplifying Inhibition of foam cells to attenuate atherosclerosis. *Adv Funct Mater*. 2021;31(46):2104892.
16. Li Z, Zhu H, Liu H, Liu D, Liu J, Zhang Y, Qin Z, Xu Y, Peng Y, Ruan L, Li J, He Y, Liu B, Long Y. Synergistic dual cell therapy for atherosclerosis regression: ROS-responsive Bio-liposomes co-loaded with Geniposide and Emodin. *J Nanobiotechnol*. 2024;22(1):129.
17. Gimbrone MA Jr, Garcia-Cardena G. Endothelial cell dysfunction and the pathobiology of atherosclerosis. *Circ Res*. 2016;118(4):620–36.
18. Sahebkar A, Banach M. Transforming hypercholesterolemia management: spotlight on PCSK9 peptide vaccines. *Cell Rep Med*. 2024;5(9):101726.
19. Wang D, Yao Y, Xiao Y, Chen X, Hu J, Yang X. Ultrasound responsive erythrocyte membrane-derived hybrid nanovesicles with controlled drug release for tumor therapy. *Nanoscale*. 2021;13(22):9945–51.
20. Lopes J, Lopes D, Pereira-Silva M, Peixoto D, Veiga F, Hamblin MR, Conde J, Corbo C, Zare EN, Ashrafizadeh M, Tay FR, Chen C, Donnelly RF, Wang X, Makvandi P, Paiva-Santos AC. Macrophage cell Membrane-Cloaked nanoplatforms for biomedical applications. *Small Methods*. 2022;6(8):e2200289.
21. Flores AM, Hosseini-Nassab N, Jarr KU, Ye J, Zhu X, Wirka R, Koh AL, Tsantilis P, Wang Y, Nanda V, Kojima Y, Zeng Y, Lotfi M, Sinclair R, Weissman IL, Ingelsson E, Smith BR, Leeper NJ. Pro-efferocytic nanoparticles are specifically taken up by lesional macrophages and prevent atherosclerosis. *Nat Nanotechnol*. 2020;15(2):154–61.
22. Qu K, Zhong Y, Zhu L, Mou N, Cao Y, Liu J, Wu S, Yan M, Yan F, Li J, Zhang C, Wu G, Zhang K, Qin X, Wu W. A macrophage Membrane-Functionalized, reactive oxygen Species-Activatable nanoprodug to alleviate inflammation and improve the lipid metabolism for atherosclerosis management. *Adv Healthc Mater*. 2024;13(26):e2401113.
23. Blanco E, Shen H, Ferrari M. Principles of nanoparticle design for overcoming biological barriers to drug delivery. *Nat Biotechnol*. 2015;33(9):941–51.
24. Lee GY, Kim JH, Choi KY, Yoon HY, Kim K, Kwon IC, Choi K, Lee BH, Park JH, Kim IS. Hyaluronic acid nanoparticles for active targeting atherosclerosis. *Biomaterials*. 2015;53:341–8.
25. Yang A, Zhang H, Zhang H, Li N, Chen C, Yang X, Tian J, Sun J, Li G, Sun Y, Liu B, Jiang Y. Pitavastatin and Resveratrol bio-nanocomplexes against hyperhomocysteinemia-induced atherosclerosis via blocking ferroptosis-related lipid deposition. *J Control Release*. 2025;381:113598.
26. Sha X, Dai Y, Chong L, Wei M, Xing M, Zhang C, Li J. Pro-efferocytic macrophage membrane biomimetic nanoparticles for the synergistic treatment of atherosclerosis via competition effect. *J Nanobiotechnol*. 2022;20(1):506.
27. Zhu L, Zhong Y, Yan M, Ni S, Zhao X, Wu S, Wang G, Zhang K, Chi Q, Qin X, Li C, Huang X, Wu W. Macrophage Membrane-Encapsulated Dopamine-Modified Poly cyclodextrin multifunctional biomimetic nanoparticles for atherosclerosis therapy. *ACS Appl Mater Interfaces*. 2024;16(25):32027–44.
28. Cao Z, Yuan G, Zeng L, Bai L, Liu X, Wu M, Sun R, Chen Z, Jiang Y, Gao Q, Chen Y, Zhang Y, Pan Y, Wang J. Macrophage-Targeted sonodynamic/photothermal synergistic therapy for preventing atherosclerotic plaque progression using CuS/TiO₂ heterostructured nanosheets. *ACS Nano*. 2022;16(7):10608–22.
29. Cochain C, Vafadarnejad E, Arampatzi P, Pelisek J, Winkels H, Ley K, Wolf D, Saliba A-E, Zernecke A. Single-Cell RNA-Seq reveals the transcriptional landscape and heterogeneity of aortic macrophages in murine atherosclerosis. *Circ Res*. 2018;122(12):1661–74.
30. Singh VK, Chau E, Mishra A, DeAnda A, Hegde VL, Sastry JK, Haviland D, Jagannath C, Godin B, Khan A. CD44 receptor targeted nanoparticles augment immunity against tuberculosis in mice. *J Controlled Release*. 2022;349:796–811.
31. Duan H, Zhang Q, Liu J, Li R, Wang D, Peng W, Wu C. Suppression of apoptosis in vascular endothelial cell, the promising way for natural medicines to treat atherosclerosis. *Pharmacol Res*. 2021;168:105599.
32. Mohamed B, Sharma I, Ibrahim AS, Saleh H, Elsherbiny NM, Fulzele S, Elmasry K, Smith SB, Al-Shabrawey M, Tawfik A. Hyperhomocysteinemia alters retinal endothelial cells barrier function and angiogenic potential via activation of oxidative stress. *Sci Rep*. 2017;7(1):11952.
33. Suhara T, Fukuo K, Yasuda O, Tsubakimoto M, Takemura Y, Kawamoto H, Yokoi T, Mogi M, Kaimoto T, Ogihara T. Homocysteine enhances endothelial apoptosis via upregulation of Fas-Mediated pathways. *Hypertension*. 2004;43(6):1208–13.
34. Zhang Y, Li JJ, Xu R, Wang XP, Zhao XY, Fang Y, Chen YP, Ma S, Di XH, Wu W, She G, Pang ZD, Wang YD, Zhang X, Xie W, Deng XL, Du XJ, Zhang Y. Nogo-B mediates endothelial oxidative stress and inflammation to promote coronary atherosclerosis in pressure-overloaded mouse hearts. *Redox Biol*. 2023;68:102944.
35. Wilkens M, Holtermann L, Stahl AK, Stegmeyer RI, Nottebaum AF, Vestweber D. Ubiquitination of VE-cadherin regulates inflammation-induced vascular permeability in vivo. *EMBO Rep*. 2024;25(9):4013–32.

36. Poels K, Schnitzler JG, Waissi F, Levels JHM, Stroes ESG, Daemen M, Lutgens E, Pennekamp AM, De Kleijn DPV, Seijkens TTP, Kroon J. Inhibition of PFKFB3 hampers the progression of atherosclerosis and promotes plaque stability. *Front Cell Dev Biol.* 2020;8:581641.
37. Doddapattar P, Dev R, Ghatge M, Patel RB, Jain M, Dhanesha N, Lentz SR, Chauhan AK. Myeloid cell PKM2 deletion enhances efferocytosis and reduces atherosclerosis. *Circ Res.* 2022;130(9):1289–305.
38. Lü S-I, Dang G-h, Deng J-c, Liu H-y, Liu B, Yang J, Ma X-I, Miao Y-t, Jiang C-t, Xu Q-b, Wang X, Feng J. Shikonin attenuates hyperhomocysteinemia-induced CD4+T cell inflammatory activation and atherosclerosis in ApoE^{-/-} mice by metabolic suppression. *Acta Pharmacol Sin.* 2020;41(1):47–55.
39. Messling JE, Agger K, Andersen KL, Kromer K, Kuepper HM, Lund AH, Helin K. Targeting R1OK2 ATPase activity leads to decreased protein synthesis and cell death in acute myeloid leukemia. *Blood.* 2022;139(2):245–55.
40. De Meyer GRY, Zurek M, Puylaert P, Martinet W. Programmed death of macrophages in atherosclerosis: mechanisms and therapeutic targets. *Nat Rev Cardiol.* 2024;21(5):312–25.
41. Katsuki S, Lupieri PKJ, Nakano A, Passos T, Rogers LSA, Becker-Greene MA, Le D, Decano TD, Ho Lee JL, Guimaraes L, Abdelhamid GC, Halu I, Muscoloni A, C A, Higashi VC, Zhang H, Vromman H, Libby A, Keith Ozaki P, Sharma C, Singh A, Aikawa SA, Aikawa E. M. Proprotein Convertase Subtilisin/Kexin 9 (PCSK9) Promotes Macrophage Activation via LDL Receptor-Independent Mechanisms. *Circ Res.* 2022;131(11):873–889.
42. Ding Z, Pothineni NVK, Goel A, Lüscher TF, Mehta JL. PCSK9 and inflammation: role of shear stress, pro-inflammatory cytokines, and LOX-1. *Cardiovascular Res.* 2019;116(5):908–15.
43. Xu S, Piao L, Wan Y, Huang Z, Meng X, Inoue A, Wang H, Yue X, Jin X, Shi GP, Kuzuya M, Cheng XW. CTSS modulates Stress-Related carotid artery thrombosis in a mouse FeCl(3) model. *Arterioscler Thromb Vasc Biol.* 2023;43(7):e238–53.
44. White LE, Cui Y, Hassoun HT, Arteriosclerosis. *Thromb Vascular Biology.* 2012;32(suppl_1):A219–219.
45. Ma C, Li Y, Tian M, Deng Q, Qin X, Lu H, Gao J, Chen M, Weinstein LS, Zhang M, Bu P, Yang J, Zhang Y, Zhang C, Zhang W. Gsa regulates macrophage foam cell formation during atherosclerosis. *Circ Res.* 2024;134(7):e34–51.
46. Xu H, She P, Zhao Z, Ma B, Li G, Wang Y. Duplex responsive nanoplatform with cascade targeting for atherosclerosis photoacoustic diagnosis and multichannel combination therapy. *Adv Mater.* 2023;35(21):2300439.
47. Zhou T, Cheng J, He S, Zhang C, Gao MX, Zhang LJ, Sun JP, Zhu Y, Ai D. The sphingosine-1-phosphate receptor 1 mediates the atheroprotective effect of eicosapentaenoic acid. *Nat Metab.* 2024;6(8):1566–83.
48. Rosenson RS, Banerjee P, Gonzaga-Jauregui C, McGinniss J, Vitali C, Pordy R, Zhao J, Ponda MP, Rader DJ. Abstract 12054: evinacumab reduces atherogenic lipids and Apolipoprotein B in patients with severe hypertriglyceridemia. *Circulation.* 2021;144(Suppl_1):A12054–12054.
49. Cai X, Liu X, Jiang J, Gao M, Wang W, Zheng H, Xu S, Li R. Molecular mechanisms, characterization methods, and utilities of nanoparticle biotransformation in nanosafety assessments. *Small.* 2020;16(36):e1907663.

Publisher's note

Springer Nature remains neutral with regard to jurisdictional claims in published maps and institutional affiliations.